The Influence of Drop Size-Dependent Fog Chemistry on Aerosol Production and Deposition in San Joaquin Valley Fogs

by

Jeffrey L. Collett, Jr. and Katherine J. Hoag
Atmospheric Science Department
Colorado State University
Fort Collins, Colorado 80523 USA

and

Spyros N. Pandis
Department of Chemical Engineering
Carnegie Mellon University
Pittsburgh, PA 15213

Research Supported by

San Joaquin Valleywide Air Pollution Study Agency
National Science Foundation (ATM-9509596)

October, 1998

Colorado State University

DEPARTMENT OF ATMOSPHERIC SCIENCE

PAPER NO. 672

The Influence of Drop Size-Dependent Fog Chemistry on Aerosol Production and Deposition in San Joaquin Valley Fogs

by

Jeffrey L. Collett, Jr. and Katherine J. Hoag
Atmospheric Science Department
Colorado State University
Fort Collins, Colorado 80523 USA

and

Spyros N. Pandis
Department of Chemical Engineering
Carnegie Mellon University
Pittsburgh, PA 15213

Research Supported by

San Joaquin Valleywide Air Pollution Study Agency
National Science Foundation (ATM-9509596)

October, 1998

Atmospheric Science Paper No. 672

DISCLAIMER

The statements and conclusions in this report are those of the Contractor and not necessarily those of the California Air Resources Board, the San Joaquin Valleywide Air Pollution Study Agency, or its Policy Committee, their employees or their members. The mention of commercial products, their source, or their use in connection with material reported herein is not to be construed as actual or implied endorsement of such products.

EXECUTIVE SUMMARY

Fog chemistry measurements in the San Joaquin Valley, including those made during the 1995 Integrated Monitoring Study (IMS95), reveal that fog drop composition varies across the drop size spectrum. Chemical heterogeneity among fog drop composition can alter aerosol processing by the fog through effects on both aqueous aerosol formation and chemical deposition.

Variations in droplet acidity and concentrations of trace metal catalysts with drop size can influence aqueous phase sulfate formation rates when oxidation is dominated by ozone and/or trace metal catalyzed autooxidation. Oxidation by ozone is enhanced by pH variations among the droplet population (Collett et al., 1994). Trace metal-catalyzed autooxidation of S(IV) can be enhanced or suppressed by variations in droplet pH and catalyst concentrations with drop size. In cases when higher than average catalyst concentrations are found in drops with higher than average pH, use of the average drop composition to predict the S(IV) oxidation rate can result in a significant underprediction of the rate of sulfate formation. By contrast, use of the average drop composition to predict S(IV) oxidation can lead to overprediction of sulfate production when catalyst concentrations and acidity are positively correlated among the droplet population. When oxidation is dominated by hydrogen peroxide, chemical heterogeneity among the fog drop population does not significantly affect sulfate production rates.

Observations of droplet composition as a function of drop size reveal that some species tend to be enriched in small drops while others are often enriched in large drops. Because droplet deposition also varies with drop size (large drops settle more quickly), the net effect is that those species enriched in large drops will be removed more quickly than predicted using average fog drop compositions, while chemical species enriched in small drops will be removed less quickly.

These issues suggest that an accurate understanding of the effects SJV fogs have on particulate matter concentrations may require knowledge about the size-dependence of

fog drop composition. However, collection of size-fractionated fog samples is much more complex and expensive than collecting bulk fog samples. If the size-dependence of SJV fog chemistry can be accurately modeled, fewer measurements of size-resolved drop composition may be necessary in future field campaigns.

APPROACH

In this project Colorado State University (CSU) and Carnegie Mellon University (CMU) collaborated to determine the effects of the drop size-dependence of fog drop composition on aerosol removal and formation during IMS95 fog events and to evaluate the CMU fog model's ability to correctly predict this size dependence.

CSU's efforts involved using observations made during IMS95 to (1) determine the dominant oxidation pathway for aqueous phase sulfate production, (2) examine the role of formaldehyde in complexing S(IV) in solution, (3) examine the effects of neglecting chemical heterogeneity among fog drop populations in favor of using the average fog drop composition to predict aqueous phase sulfate production rates, and (4) examine the effect of non-uniform distributions of solute concentrations with drop size on predictions of solute removal rates via fog droplet settling. These tasks combine the efforts for CSU's work on IMS95 data analysis tasks 4.6.4 and 4.6.7. Because of the natural overlap between CSU's work on these tasks, we choose to present all of the results in this report.

CMU conducted model simulations of IMS95 fog episodes using multiple versions of their radiation fog model. Predictions of a size-resolved fog chemistry version of the model were compared to CSU's observations of size-dependent fog chemistry during IMS95 to evaluate the ability of the model to realistically simulate chemical heterogeneity among SJV fog drop populations. Simulations using the size-resolved fog chemistry model were then compared to simulations using a bulk fog chemistry version of the model to determine the effects size-dependent fog chemistry has on aerosol production and removal during a Fresno IMS95 fog event.

Results from the complementary analyses conducted by CMU and CSU were then integrated. Based on our findings, we recommend a strategy for characterizing aerosol processing by chemically heterogeneous fogs in a future San Joaquin Valley particulate matter study.

MAJOR CONCLUSIONS AND RECOMMENDATIONS

As a result of the data analysis conducted during this project a number of conclusions have been reached and a set of recommendations made. General conclusions and recommendations are listed with square bullets. Those dealing specifically with the issue of drop size-dependent fog composition are listed in bold with round bullets.

- Direct analysis of the fog chemistry and microphysics observations indicates that aqueous sulfate formation is an important phenomenon in SJV fogs. Despite low ozone concentrations observed in conjunction with the fog events, calculations of expected oxidation rates in the collected fog samples reveal ozone to be the most important oxidant for sulfate production in the fogs. Ozone was determined to be the leading S(IV) oxidant in 98% of the study samples with a pH greater than 6.0.
- Temporal analysis of sulfate production rates in the fogs indicates there is no general decline in oxidation rates over the course of an episode. Although one expects the drops to acidify rapidly as S(IV) is oxidized to sulfuric acid, accompanied by a precipitous decline in the rate of S(IV) oxidation by ozone, enough buffering capacity is apparently present in the system to keep droplet pH values relatively high.
- **Observations of fog composition during IMS95 reveal that droplet composition varies with drop size. All inorganic ion species measured were enriched in small drops relative to their large drop concentrations. Small drops were also consistently more acidic than large drops, although both large and small drops were generally at a high pH relative to fog or cloud drops found in most environments.**
- **Tests of the size-resolved fog chemistry model of CMU revealed its ability to predict size-dependent fog drop compositions in close agreement with IMS95**

observations made by CSU. Although further comparisons should be made, requiring collection of additional data sets, these initial comparisons are quite encouraging and support the use of the model as a tool for investigating the role of SJV fogs as aerosol processors.

- Because the rate of aqueous S(IV) oxidation by ozone depends nonlinearly on the hydrogen ion concentration, it is inaccurate to predict sulfate formation rates in these fogs based on average droplet acidity. Calculated sulfate formation rates using observations of size-dependent drop chemistry reveal that an assumption of chemical homogeneity among the fog drop population leads to an underestimation of the oxidation rate by as much as a factor of nine.
- Enrichment of ion concentrations in small drops, which settle to the ground only slowly, appears capable of reducing aerosol removal rates via droplet sedimentation relative to values one would predict from average droplet composition. It is difficult to make strong conclusions about this effect from fog chemistry observations without having better drop size resolution in the fog chemistry measurements.
- Model simulations indicate that the sulfate produced during fog episodes favors the aerosol particles that have access to most of the fog liquid water, which are usually the large particles. Nitrate, by contrast is associated more strongly with small fog drops. The size distribution of ammonium in the fog drops is predicted to exhibit a bimodal nature vs. drop size as ammonia is absorbed from the gas phase to neutralize acidity associated with the nitrate and sulfate.
- Model simulations yield aerosol scavenging efficiencies of around 60% for SJV fogs during IMS95.
- Simulation of the extended fog event of December 10, 1995 indicated the fog contributes substantially to removal of ammonium and nitrate from the boundary layer. Removal of sulfate competes with aqueous-phase production throughout the fog episode resulting in a net increase of 60% in sulfate concentration. Sulfate production in the model is dominated by the ozone and hydrogen peroxide pathways.

- **Simulation of the size-dependent fog drop composition results in a sulfate concentration that is 30% higher than predicted by a bulk fog model simulation of the same episode.**
- While measured ozone concentrations during IMS95 fog episodes were typically a few ppb, model simulations suggest the ozone should be consumed at night by reaction with NO. Given the sensitivity of the sulfate production to ozone concentrations, it is strongly recommended that future studies of aerosol processing by fogs in the SJV carefully evaluate the accuracy of ozone measurements at levels below 5 ppb.
- **Sampling and subsequent mixing of fog droplets of different sizes may result in measured concentrations that are not fully representative of the fogwater chemical composition and can introduce errors in the reported values of the ionic species deposition velocities. Differences in the observed major ionic species deposition velocities (ammonium > sulfate > nitrate) can be explained by their distribution over the fog drop size spectrum.**
- **Because the effects of size-dependent drop composition are so important to aerosol formation and removal in SJV fogs, it is recommended that future studies of winter particulate matter processing by SJV fogs consider this issue further.**
- **The encouraging agreement between model simulations and size-resolved fog chemistry observations suggest that a wise use of resources would be to make detailed measurements of size-resolved fog drop composition at a core location and rely on simpler measurements at other sites.**
- **With recent advances in technology for measuring size resolved fog, we recommend that greater drop size resolution (at least 5 independent size fractions can now be collected for chemical analysis) be used for size-resolved drop chemistry measurements at a core site in a future SJV winter particulate matter study. These measurements should be accompanied by high time resolution fog drop size distribution and fog liquid water content measurements to test the model's simulation of fog microphysics and by fog deposition**

measurements to help constrain model simulations of solute flux to the ground via droplet sedimentation.

- **In order to properly simulate the size-resolved fog chemistry, it is important that pre-fog measurements of the size-dependent aerosol composition (e.g., with a MOUDI or Berner impactor) also be made at the core fog measurement site.**
- **One or two additional satellite sites should be equipped with easy-to-operate two stage fog collectors. If resources permit, it would be wise to add additional, automated sites employing single-stage strand collectors. If these stations were configured to collect one sample per fog event, several could be serviced by a roving fog operator that would visit the sites once per day. Such sites would provide information about spatial variations in fog composition that were not examined during IMS95 (e.g., does fog along the western valley slope remain considerably more acidic than fog in the center of the valley, as observed during SJV fog studies conducted in the early 1980's).**

1. Introduction

Historically, urban fogs have frequently been interconnected with severe pollution episodes (Wilkins, 1954). A cyclical relationship between the occurrence of smog and fog in the Los Angeles basin has been proposed by Munger et al. (1983) and was termed the smog-fog-smog cycle. A polluted atmosphere with high aerosol concentration assists the formation of late night and early morning fogs which appear to enhance smog production, visibility reduction, and aerosol sulfate levels during the following day.

Fogs can be viewed as physicochemical processors of the ambient aerosol and of various gaseous pollutants. As the relative humidity of an air parcel, in contact with the ground, increases, water condenses on the aerosol particles in accordance with water vapor equilibrium. If the relative humidity of the parcel reaches a critical supersaturation, the value of which depends on the size and chemical composition of the aerosol present, the particles become activated, grow freely by vapor diffusion, and a fog forms. The growth of the aerosol particles to liquid droplets leads to the acceleration of particle removal from the atmosphere decreasing in this way the aerosol concentration. Soluble gaseous species such as nitric acid, sulfur dioxide, and ammonia are transferred to the aqueous phase and their deposition is also enhanced. At the same time the fog formation provides the reacting medium, the liquid water, for aqueous-phase reactions. Several species dissolve in fogwater and react giving products that remain in the aerosol phase after the fog dissipates, for example the dissolution of SO_2, its ionization and its subsequent oxidation to sulfate. These species can attract additional gaseous species, for example ammonia and water, into the aerosol phase and therefore a fog may also increase the aerosol mass.

Fog chemistry measurements in the San Joaquin Valley, including those made during IMS95, reveal that fog drop composition varies across the drop size spectrum. Chemical heterogeneity among fog drop composition can alter aerosol processing by the fog through effects on both aqueous aerosol formation and chemical deposition.

Variations in droplet acidity and concentrations of trace metal catalysts with drop size can influence aqueous phase sulfate formation rates when oxidation is dominated by ozone and/or trace metal catalyzed autooxidation. Oxidation by ozone is enhanced by pH variations among the droplet population (Collett et al., 1994). Trace metal-catalyzed autooxidation of S(IV) can be enhanced or suppressed by variations in droplet pH and catalyst concentrations with drop size. In cases when higher than average catalyst concentrations are found in drops with higher than average pH, the enhancement can be significant. Oxidation suppression occurs when catalyst concentrations and acidity are positively correlated. When oxidation is dominated by hydrogen peroxide, chemical heterogeneity among the fog drop population does not significantly affect sulfate production rates.

Observations of droplet composition as a function of drop size reveal that some species tend to be enriched in small drops while others are often enriched in large drops. Because droplet deposition also varies with drop size (large drops settle more quickly), the net effect is that those species enriched in large drops will be removed more quickly than predicted using average fog drop compositions, while chemical species enriched in small drops will be removed less quickly. Previous field measurements in the SJV have indicated that fog deposition velocities of different ionic species can be quite different (Waldman, 1986). This is consistent with the observations of variations in solute mass across the drop size spectrum. Pandis et al. (1990a) explained these observations with a drop size-resolved fog model.

These issues suggest that an accurate understanding of the effects SJV fogs have on particulate matter concentrations may require knowledge about the size-dependence of fog drop composition. However, collection of size-fractionated fog samples is much more complex and expensive than collecting bulk fog samples. The instrumentation required is more expensive (and not widely available), the work in the field is much more labor intensive, more supplies are required, and there are more samples to analyze. In order to determine whether the additional effort of size-fractionated droplet sampling is warranted for future work in the region, there is clearly a need to evaluate how significant

the effect of non-uniform droplet compositions is on aerosol formation and deposition in fog events. It is also desirable to test the ability of numerical models to correctly predict the size-dependent composition. If this phenomenon can be accurately modeled, fewer measurements of size-resolved drop composition may be necessary in future field campaigns.

In this project Colorado State University (CSU) and Carnegie Mellon University (CMU) collaborated to determine the effects of the observed drop size-dependence of fog drop composition on aerosol removal and formation during IMS95 fog events and to evaluate the CMU model's ability to correctly predict this size dependence. Based on our findings, we recommend a strategy for characterizing aerosol processing by chemically heterogeneous fogs in a future San Joaquin Valley particulate matter study.

2. Analysis of Experimental Results

One objective of this data analysis task was to utilize experimental observations of size-dependent fog drop composition to determine rates of aerosol solute formation and deposition during the fog events studied in IMS95. In task 4.6.4 CSU also used experimental observations of bulk fog chemistry to calculate rates of S(IV) oxidation and to examine the relative importance of S(IV) complexation by formaldehyde. Because these tasks are related, we present results from these particular 4.6.4 data analysis tasks in this report. We begin by looking at S(IV) oxidation and aldehyde complexation in bulk fog samples collected during IMS95 and then examine oxidation and deposition processes in drop size-resolved fog samples.

2.1 S(IV) Oxidation

SO_2, a major gaseous primary pollutant, is absorbed by fog drops and is one of the major contributors to aqueous phase atmospheric chemistry. In its aqueous form, SO_2 is partitioned into H_2SO_3, HSO_3^- and SO_3^{2-}. This partitioning tends toward sulfite (SO_3^{2-}) at high pH, allowing more SO_2 into the droplet. Conversely, if the drop pH falls, the equilibrium tends toward H_2SO_3, limiting further absorption of $SO_{2(g)}$.

Once in aqueous form SO_2 (S(IV)) oxidizes readily to H_2SO_4 (S(VI)). There are three main oxidation pathways corresponding to different oxidants: hydrogen peroxide, ozone and oxygen. The oxygen pathway is catalyzed by Fe(III) and Mn(II), metals commonly found in atmospheric particles upon which fog drops form. Previous studies usually focused on S(IV) oxidation by the hydrogen peroxide pathway, since with ample amounts of all oxidants and catalysts, this pathway would be dominant at the lower pH range usually seen in atmospheric water. However, the H_2O_2 pathway is pH independent over a pH range from 2 to 8, while the other two oxidation pathways are very pH dependent, their rates increasing dramatically with increasing pH (see Fig 2.1). Therefore, in less acidic fogs, the oxidation process must be examined more carefully to determine dominant mechanisms.

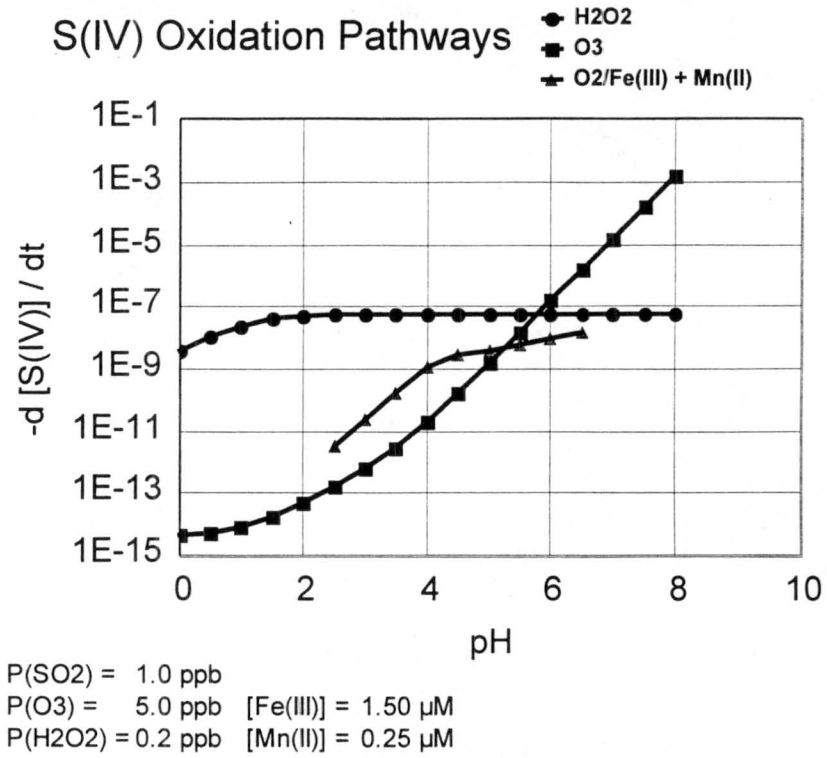

Figure 2.1. S(IV) oxidation rates as a function of pH for typical San Joaquin Valley conditions. Increases of SO_2 would shift all curves together, whereas increases in individual oxidant or catalyst concentrations would shift only the pertaining rate curve. (H_2O_2: Seinfeld, 1986; O_3: Hoffmann, 1986; O_2/Fe(III)+Mn(II): Ibusuki and Takeuchi, 1987) Rates are given in **M** s^{-1}.

The following equations are used for S(IV) oxidation rate calculations (all concentrations are in units of **M** and rate constants are given for 10°C, representative of the general conditions during the fog events):

H_2O_2:

$$-d[S(IV)]/dt = k\,[H^+]\,[H_2O_2]\,[HSO_3^-] / (1+13[H^+]) \quad (1)$$

where k = 3.20 E+7 $M^{-1}s^{-1}$, (Seinfeld, 1986).

O_3:

$$-d[S(IV)]/dt = [O_3](k_1[H_2SO_3] + k_2[HSO_3^-] + k_3[SO_3^{2-}]) \quad (2)$$

where k_1 = 2.4 E+4 $M^{-1}s^{-1}$, k_2 = 1.4 E+5 $M^{-1}s^{-1}$, and k_3 = 5.9 E+8 $M^{-1}s^{-1}$, (Hoffmann, 1986).

O_2/Fe(III)+Mn(II) (4.2 < pH < 6.5):

$$-d[S(IV)]/dt = k\,[Fe(III)]\,[Mn(II)]\,[S(IV)]\,[H^+]^{0.67} \quad (3)$$

where k = 6.3 E+12 $M^{-1}s^{-1}$ (Ibusuki and Takeuchi 1987). This rate expression was also applied to samples whose pH was above 6.5 due to the lack of other experimental rate results for relevant concentrations including the synergistic effect between iron and manganese.

2.2 S(IV) Oxidation Rate Calculations in Bulk Fog Samples

Measured fog pH values and measured metals concentrations were used in the calculations. Dissolved Fe(III) was assumed to comprise one quarter of the total aqueous iron concentration. Henry's Law (constants at 10°C) was used to obtain aqueous O_3, H_2O_2, and SO_2 concentrations from measured gas concentrations averaged over relevant sampling times. The speciation of $SO_{2(aq)}$ was calculated at 10°C. When gas concentrations were below the lowest quantifiable level (LQL) of the instrument the concentration of the gas was assumed to be the LQL. When data were unavailable for SO_2 or O_3, concentrations at the corresponding time period on preceding or subsequent days were used. In cases when H_2O_2 data were missing, concentrations were taken from an average diurnal pattern calculated as an average for each hour of the day for all study days. This was done because large variability in the data made it difficult to determine a representative daily pattern from one day of data alone. Figure 2.2 shows histograms of the sulfur dioxide, ozone, and hydrogen peroxide gas phase concentrations (including actual measurements and estimated values) used in the S(IV) oxidation calculations.

At the tower, gases were measured at the ground and at the top of the tower (430 m), while two of the samplers were located in between these elevations. Gas concentrations

for intermediate elevations on the tower were estimated by assuming a linear profile of each gas between the ground and top of the tower. Figure 2.3 shows the histograms of the gas concentrations used for the S(IV) oxidation calculations for the samples collected at the tower. It is clear that SO_2 levels are fairly low, but O_3 and H_2O_2 levels are fairly high compared to the southern SJV urban sites.

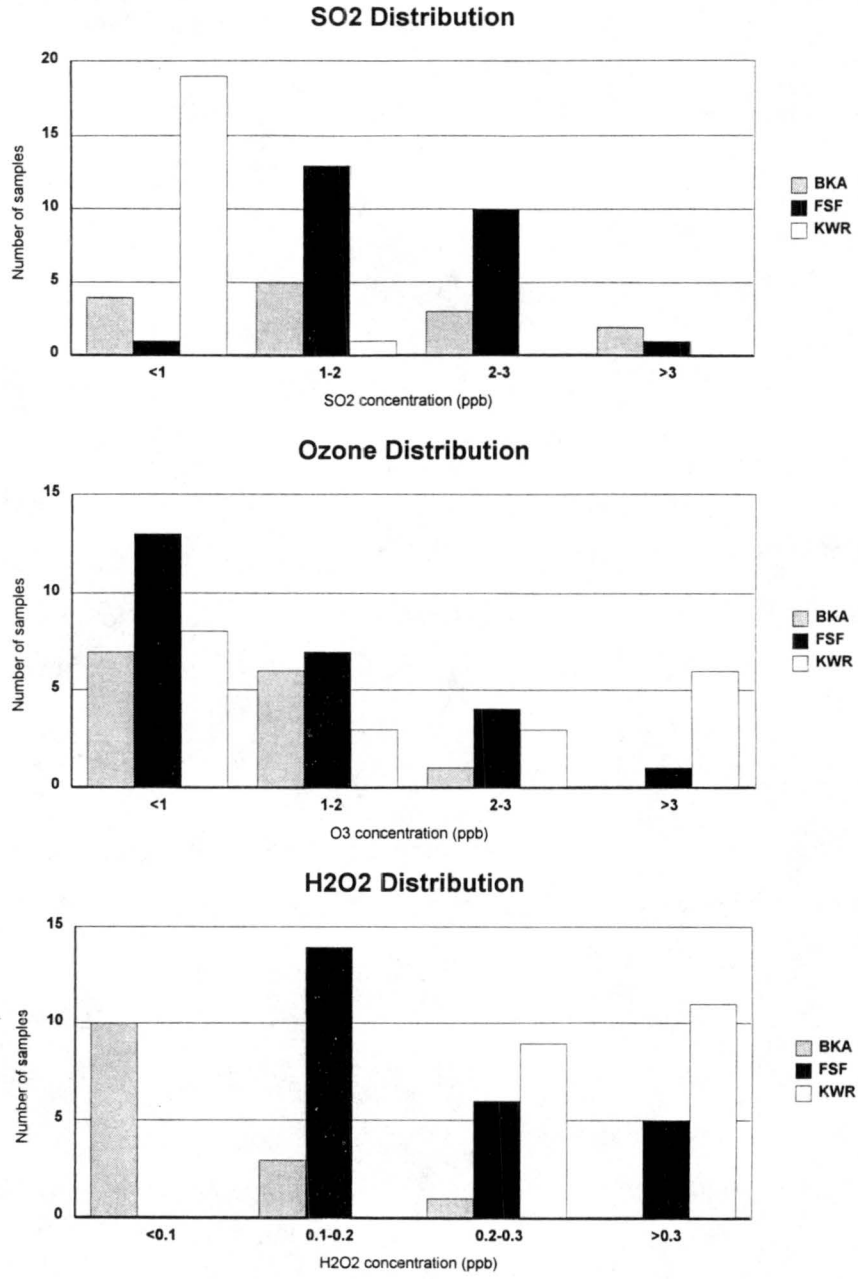

Figure 2.2. Gas phase concentrations of sulfur dioxide, ozone and hydrogen peroxide used in the S(IV) oxidation calculations.

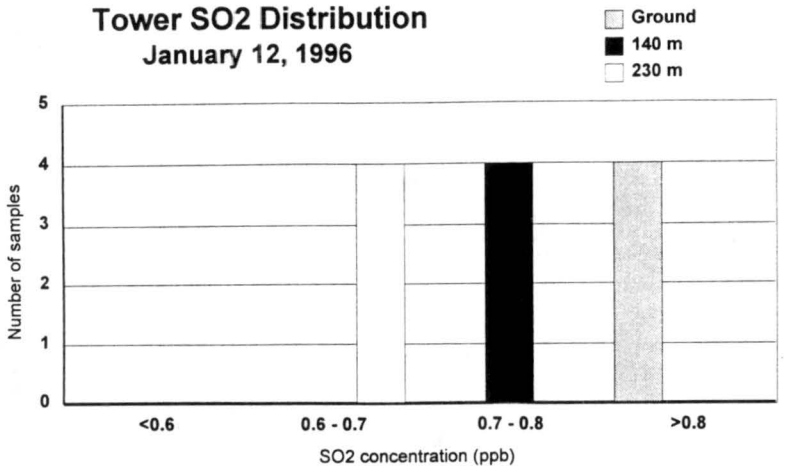

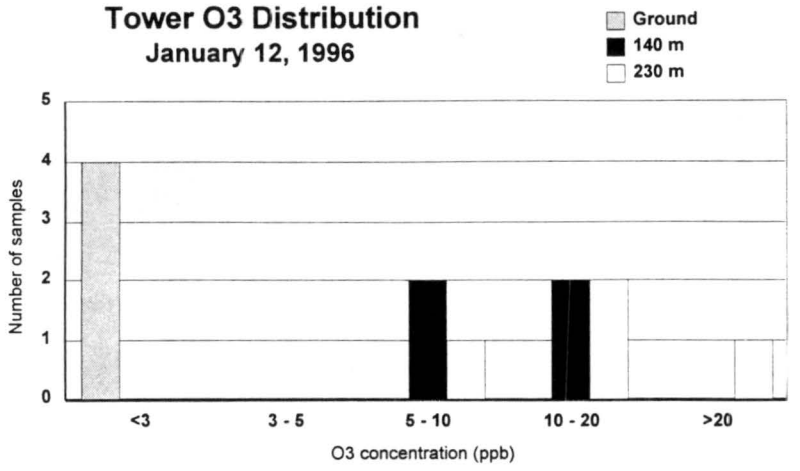

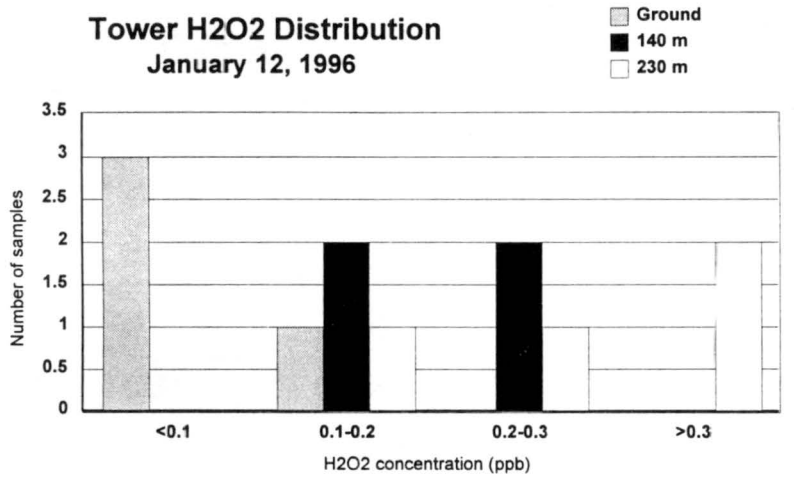

Figure 2.3. Gas concentrations used for January 12 oxidation calculations at the Candelabra Tower. Gases were collected at the ground and 430 m, and linear vertical profiles were assumed.

The results of the S(IV) oxidation rate calculations for the first two southern SJV events (12/9 and 12/10/95) and for one tower event (1/12/96) are shown in Figures 2.4-2.7. It is clear that in most cases the ozone pathway is fastest, often by an order of magnitude or more.

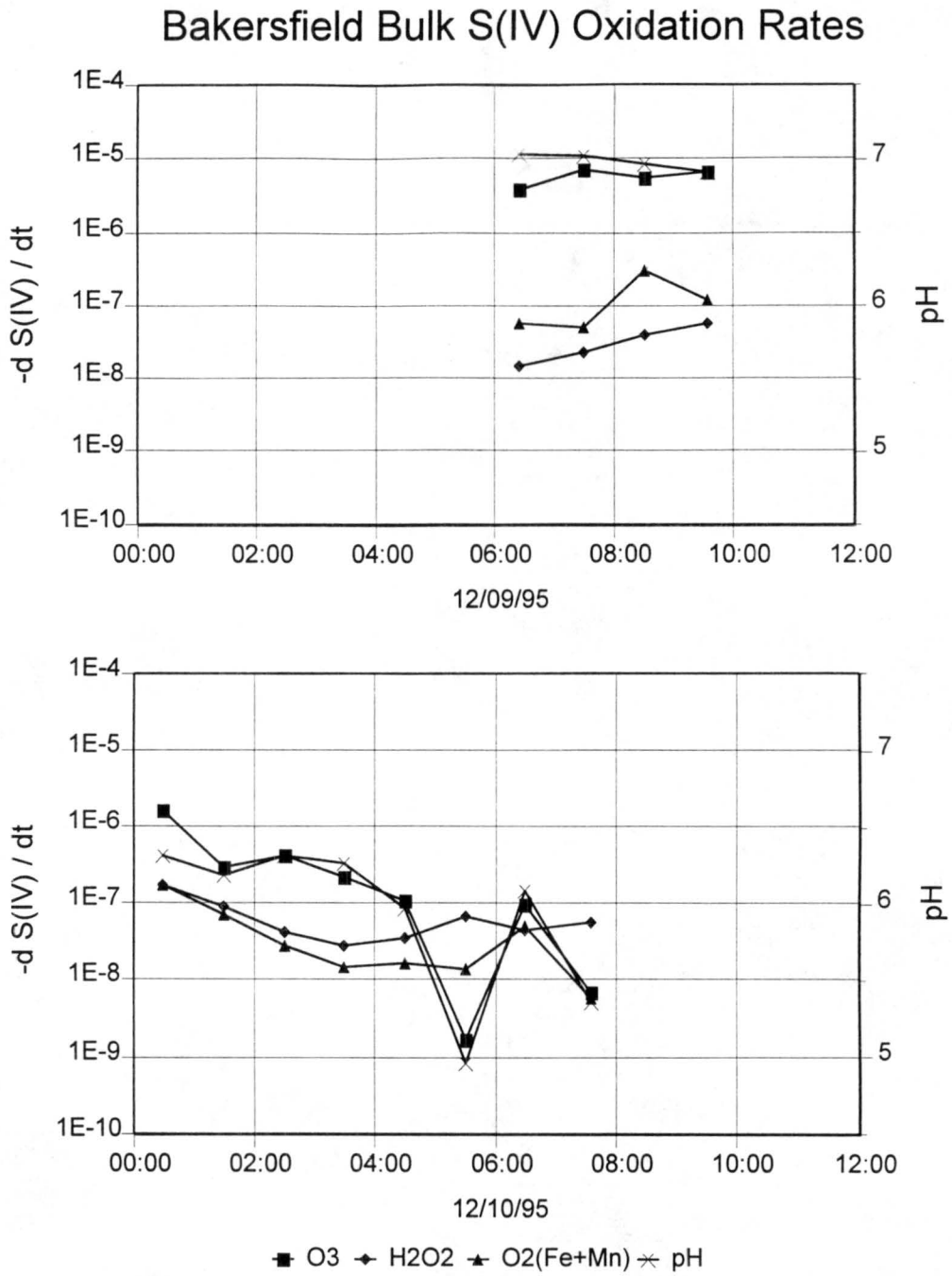

Figure 2.4. S(IV) oxidation rates calculated for bulk samples collected at Bakersfield as functions of time. Field pH values are also plotted for each sample. Rates are given in **M** s^{-1}.

At Bakersfield S(IV) oxidation rates were dominated by ozone, with some samples having hydrogen peroxide as the primary oxidant. The cases where the peroxide pathway was faster (samples #6 and #8 on 12/10/95) also exhibited lower than average pH values. S(IV) and sulfate concentrations were also very elevated in these samples. The significantly lower pH allows the H_2O_2 oxidation pathway to dominate over the O_3 pathway, which slows at lower pH.

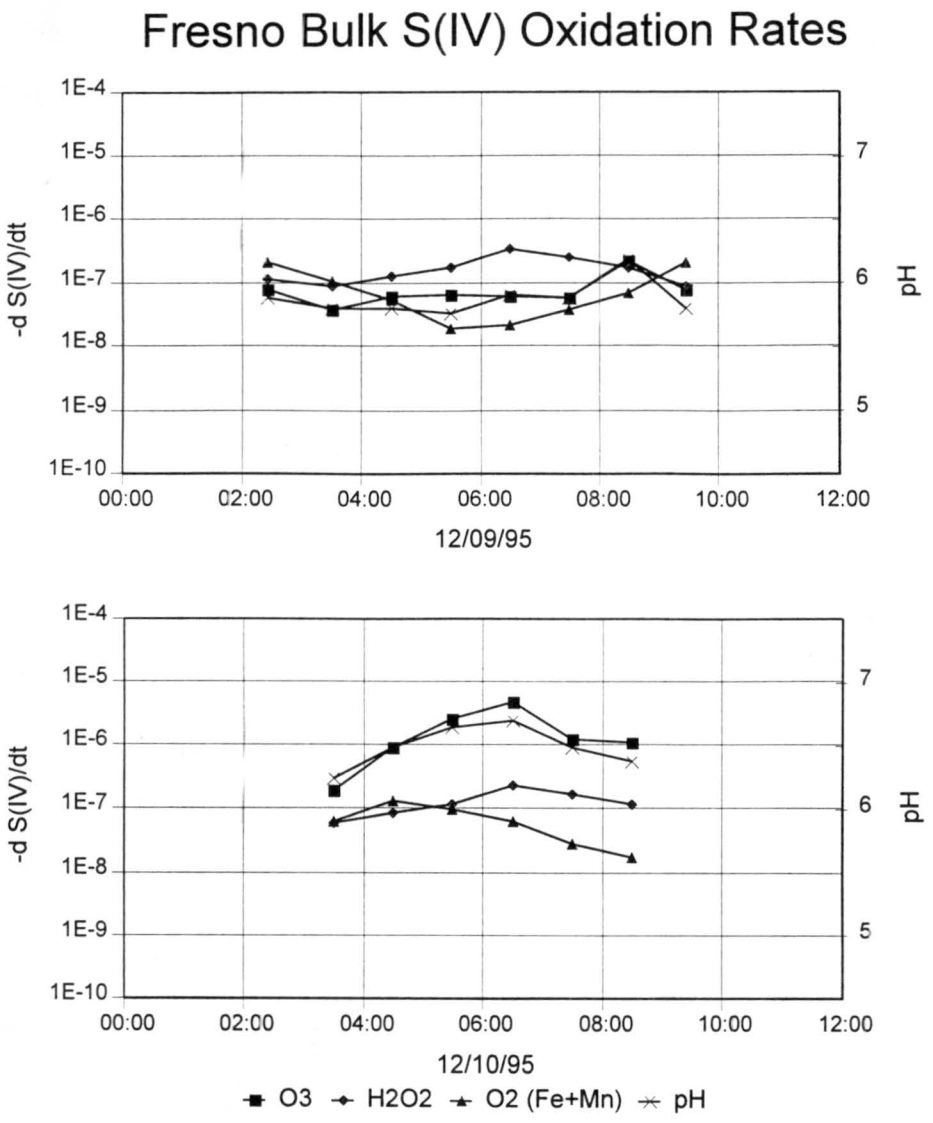

Figure 2.5. S(IV) oxidation rates calculated for bulk samples collected at Fresno as functions of time. Field pH values are also plotted for each sample. Rates are given in **M** s^{-1}.

At Fresno, the fog events on December 10, 19, 28 and January 4 all had a high enough pH so that ozone is the primary S(IV) oxidant. On December 9, different oxidants dominated in different samples. At the beginning and end of the event, high iron and manganese values along with a pH below 6 allowed metal catalyzed autooxidation to be fastest. During the middle of the event, the metals concentrations are lower and the peroxide pathway dominates except for one sample with a pH above 6, for which the ozone pathway is fastest. During the January 1 event, metals concentrations are very low and the pH of the fog remains around 6 so that at different times ozone or hydrogen peroxide are the primary oxidant. For the first and last samples of this event, the peroxide and ozone rates are within 10 percent of each other so both are important. Since gas concentrations are fairly constant over the events at Fresno, it seems that high metals concentrations and low pH values are necessary for the metal catalyzed autooxidation pathway to dominate, and that the peroxide pathway is usually dominant for $pH \leq 6$.

Fogs sampled at Kern Wildlife Refuge tended to be less acidic than the other two southern sites and the ozone pathway was always fastest. This was also true at the Candelabra Tower, where fog pH values provide conditions in which the ozone pathway was always at least an order of magnitude faster than the peroxide pathway and metal catalyzed autooxidation is much slower still.

Generally, oxidation rates are comparable between the three southern sites, only slightly higher at Kern and the tower due to the higher fog pH observed there. In most cases, oxidation rates were also fairly constant with time throughout the fog event, suggesting that oxidation did not cease over time due to the acidification of the drops. In fact, even when significant pH decreases occurred (Bakersfield, December 10), the peroxide pathway becomes important and the overall S(IV) oxidation rate remains fairly constant.

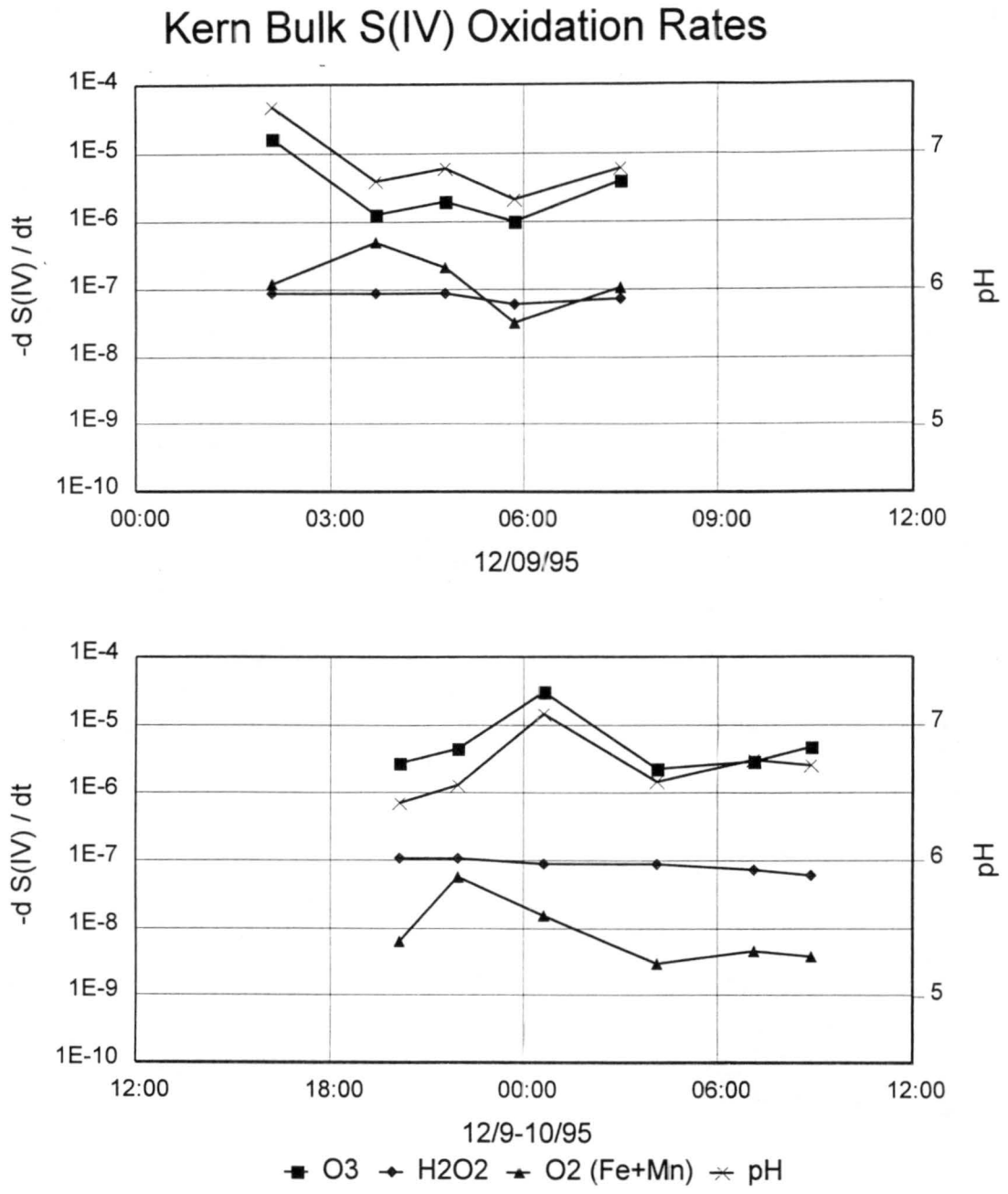

Figure 2.6. S(IV) oxidation rates calculated for bulk samples collected at Kern Wildlife Refuge as functions of time. Field pH values are also plotted for each sample. Rates are given in **M** s^{-1}.

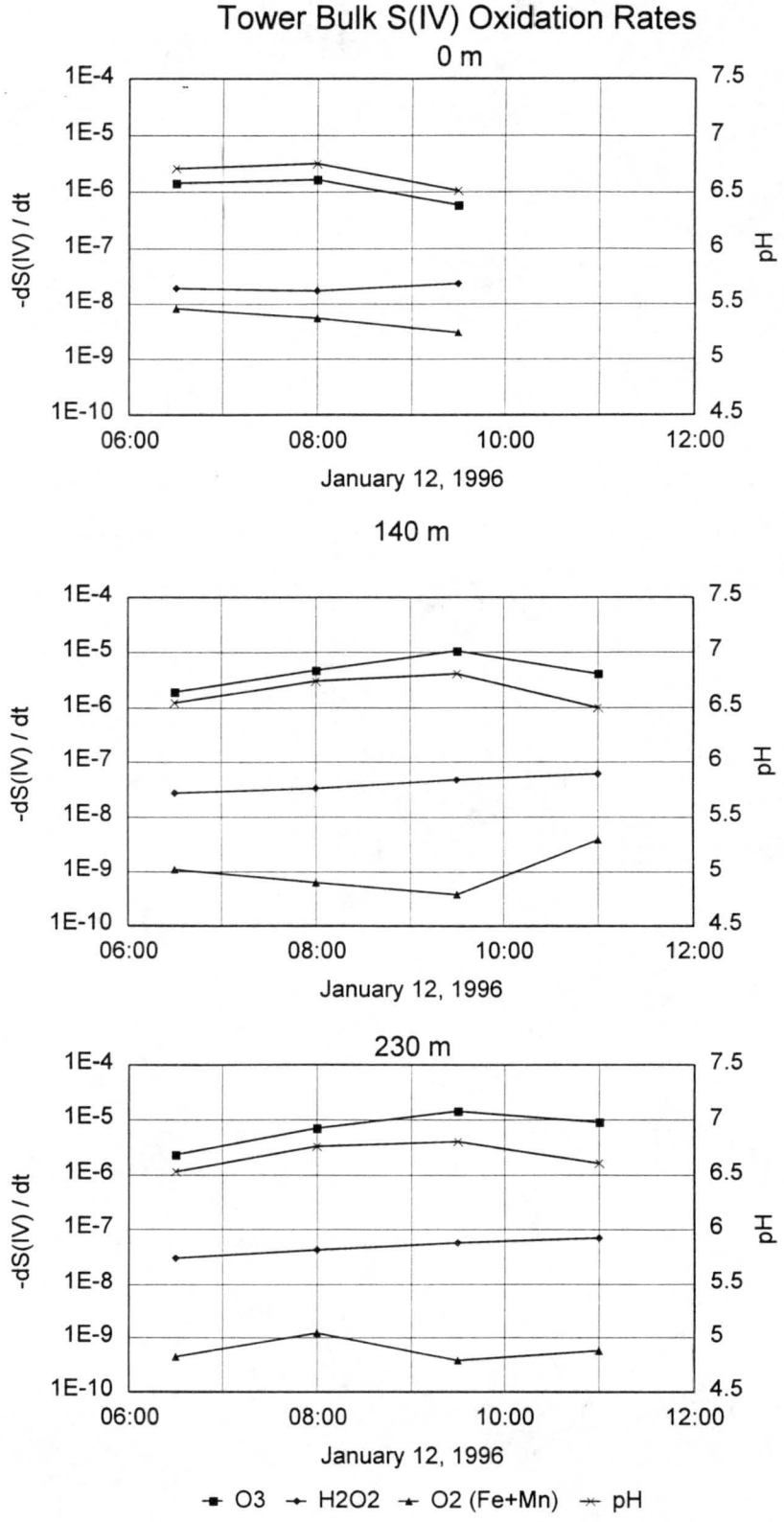

Figure 2.7. S(IV) oxidation rates calculated for bulk samples collected at the ground and two elevations on the Candelabra Tower as functions of time. Field pH values are also plotted for each sample. Rates are given in **M** s^{-1}.

Figure 2.8 shows the percentage of time that each of the S(IV) oxidation pathways is dominant (at least 10 percent faster than competing pathways) for each of the IMS95 fog sites for all of the events sampled. The ozone S(IV) oxidation pathway is dominant 85 percent of the time at Bakersfield, 60 percent at Fresno and during every event sampled at Kern. The ozone pathway is also dominant at each elevation during every event sampled at the Candelabra Tower. Overall, in the southern SJV fogs sampled during IMS95, ozone was the leading oxidant of aqueous S(IV) 88 percent of the time, peroxide 8 percent of the time and oxygen 3 percent of the time. During 1 percent of the time, both ozone and hydrogen peroxide were important oxidants and the oxidation rates of these pathways were within 10 percent of each other. These numbers change little if we alter the criteria so that an oxidation pathway must be 50 percent faster than the next fastest pathway to be considered dominant. In this case ozone is determined to be the dominant oxidant in southern SJV fogs 86 percent of the time, hydrogen peroxide dominates 7 percent of the time and oxygen dominates 2 percent of the time. During 4 percent of the time the ozone and hydrogen peroxide rates are within 50 percent of each other. During 1 percent of the time the hydrogen peroxide rates are fastest and within 50 percent of each other.

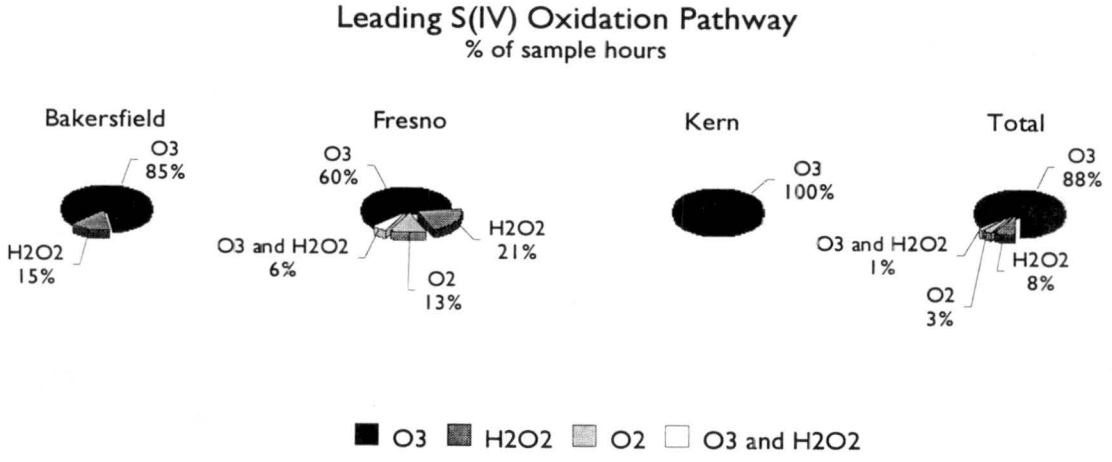

Figure 2.8. Leading S(IV) oxidation pathways for each southern SJV site and all three sites combined (total). The percentages represent the fraction of sampling hours that the designated pathway was at least 10% faster than the other pathways. The 'O_3 and H_2O_2' fraction represents periods of the fog when both the ozone and peroxide S(IV) oxidation path were important and within 10% of each other.

It is even more remarkable that ozone is dominating these chemical processes when the low ozone concentrations are considered. The observed concentrations of ozone, particularly during the fog episodes are much lower than typical background tropospheric values (20-40 ppbv). SJV ozone is depleted at night by reaction with the abundant NO resulting in formation of nitrogen dioxide which, in the absence of sunlight, cannot be photolyzed to regenerate ozone. Additional ozone loss may be due to consumption via aqueous phase processes.

A clear pattern is seen if the leading pathway is considered in light of the sample pH. Table 2.1 breaks down the leading pathway for three pH ranges. Above a sample pH of 6.0, S(IV) oxidation by ozone is fastest for 98 percent of the samples collected. Samples with pH values between 5.5 and 6.0 exhibit more of a range of various leading S(IV) oxidation pathways. In these cases, a higher oxidant or catalyst concentration is likely to determine the fastest pathway. There are only two samples with pH below 5.5, and S(IV) oxidation by H_2O_2 is fastest for both. Since the ozone pathway depends on $[H^+]$ nonlinearly and the peroxide pathway is relatively independent of $[H^+]$, the chemistry occurring with ozone as the primary oxidant will differ significantly from peroxide dominated environments. Therefore, as will be shown in the next section, observed differences in the fog acidity as a function of drop size will greatly affect the total in-fog sulfate production since it is governed by a nonlinear reaction with respect to $[H^+]$.

Table 2.1: The percent of samples in three pH ranges where each S(IV) oxidation pathway is fastest.

pH	# of samples	% O_3	% H_2O_2	% O_2 / Fe(III)+Mn(II)	% O_3 and H_2O_2 *
> 6.0	47	98	2	0	0
5.5 - 6.0	10	10	40	30	20
< 5.5	2	0	100	0	0

* rates within 10 % of each other

2.3 Sensitivity Analysis of Bulk S(IV) Oxidation

Calculations were performed to determine the sensitivity of the S(IV) oxidation calculations to oxidant and catalyst concentrations. Rates were determined with half the O_3, twice the H_2O_2, four times the Fe(III) and two times the Mn(II) concentrations used in the original calculations. These factors represent upper bounds on the gas concentration and metals speciation uncertainties that would tend toward making O_3 a less important pathway. Calculations were also made taking each of these conditions into account separately. Figure 2.9 shows the results of applying all the sensitivity tests at once. It is clear that these conditions decrease the importance of the ozone oxidation pathway at Fresno and Bakersfield primarily through an increase of the importance of the autooxidation pathway. Kern oxidation rates were affected only slightly by all the changes.

Figure 2.10 shows the leading pathways when oxidation calculations are performed taking into account changes in ozone, hydrogen peroxide or the metals concentrations separately, in addition to the case in which ozone concentrations are doubled. In each case, particularly when metals concentrations are altered, samples collected at Bakersfield

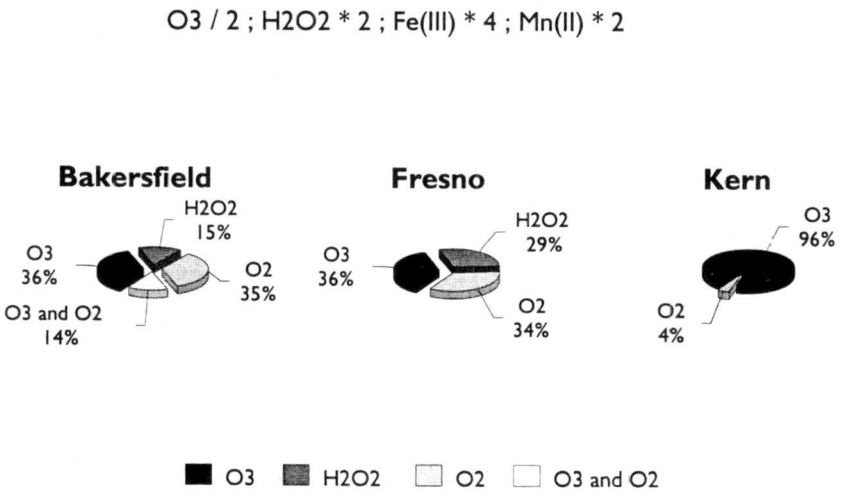

Figure 2.9. Sensitivity tests showing dominant S(IV) oxidation pathways for each southern SJV site and all three sites for conditions tending to minimize the importance of S(IV) oxidation by ozone.

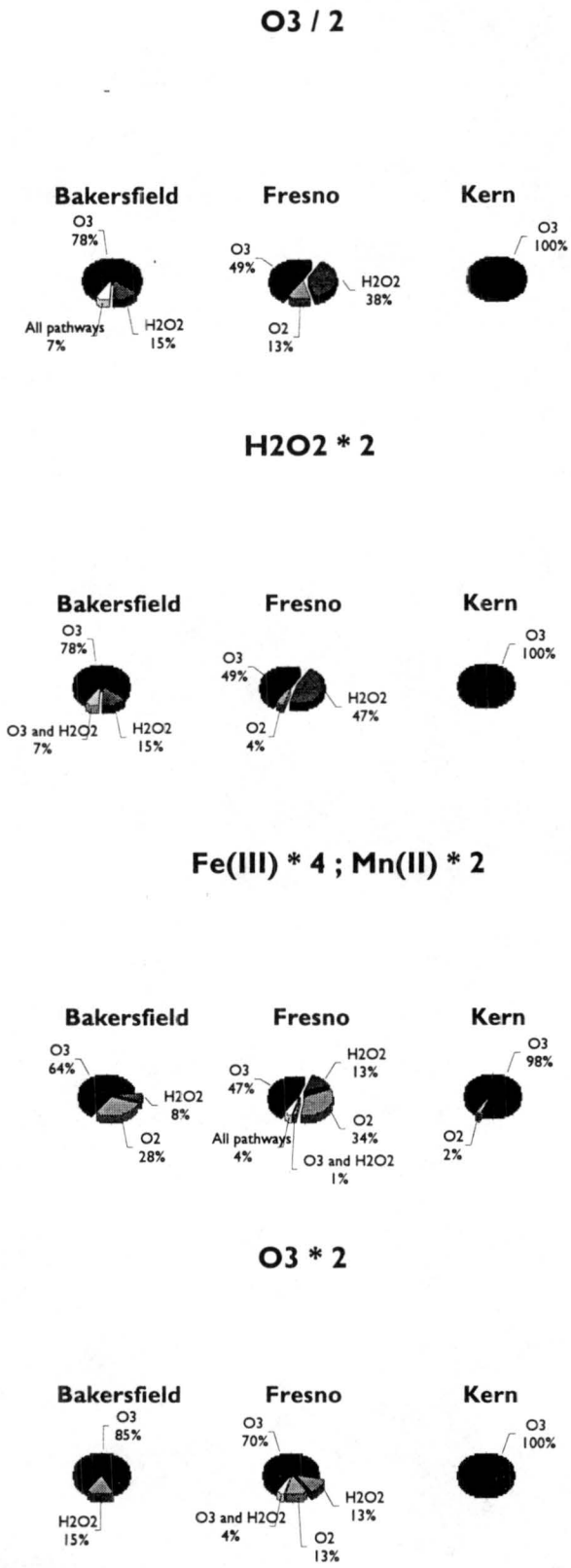

Figure 2.10. Leading pathways calculated for each of the sensitivity conditions (and doubling ozone) separately.

and Fresno exhibit major changes in the percent of time that each pathway is fastest (decreasing the amount of time ozone is the primary oxidant). Conversely, at Kern, the ozone pathway remains fastest regardless of altering O_3 or H_2O_2 alone, and decreases negligibly when the metals concentrations are raised. When ozone concentrations are doubled, the leading pathways at Bakersfield and Kern remain the same as when calculated with initial concentrations and the ozone mechanism increases the fraction of time it is leading by 10 percent at Fresno at the expense of the peroxide pathway. These calculations show that oxidant concentrations and particularly the metals concentrations are important to know accurately for precise determinations of the in-fog sulfate production.

Model simulations of these fog episodes by Carnegie Mellon University have suggested that sufficient NO is present to titrate the ozone to zero at night. Accordingly, S(IV) oxidation rates were recalculated for two cases. Case one assumed ozone to be zero when the data were below the lower quantitation limit (LQL), and case two assumed there was no ozone throughout the entire study. Tables 2.2-5 show the results of these calculations for each site. For case one, the importance of S(IV) oxidation by ozone decreases at Bakersfield leading to an increasing importance of the autooxidation pathway. At Fresno and Kern a decrease in the importance of ozone led to an increase in the importance of the peroxide pathway. The tower S(IV) oxidation rates exhibited no change since all ozone values there were above the LQL. At the three southern sites, the importance of both the peroxide and autooxidation pathways were increased significantly in the absence of ozone (case two), whereas at the tower the peroxide pathway was always fastest. In the absence of ozone, the total S(IV) oxidation rates are often an order of magnitude slower than when it is present. This would lower the amount of sulfate the fog could produce.

Table 2.2. Comparison of leading S(IV) oxidation pathways at Bakersfield, considering ozone to be absent when below the LQL and throughout the entire event.

Sensitivity Conditions	% O_3	% H_2O_2	% O_2 / Fe(III)+Mn(II)	% O_3 and H_2O_2 *	% H_2O_2 and O_2 *
Original	85	15	0	0	0
O3 = 0 below LQL	78	15	7	0	0
No O3	0	50	36	0	14

Table 2.3. Comparison of leading S(IV) oxidation pathways at Fresno, considering ozone to be absent when below the LQL and throughout the entire event.

Sensitivity Conditions	% O_3	% H_2O_2	% O_2 / Fe(III)+Mn(II)	% O_3 and H_2O_2 *	% H_2O_2 and O_2 *
Original	60	21	13	6	0
O3 = 0 below LQL	49	32	13	6	0
No O3	0	78	17	0	4

Table 2.4. Comparison of leading S(IV) oxidation pathways at Kern, considering ozone to be absent when below the LQL and throughout the entire event.

Sensitivity Conditions	% O_3	% H_2O_2	% O_2 / Fe(III)+Mn(II)	% O_3 and H_2O_2 *	% H_2O_2 and O_2 *
Original	100	0	0	0	0
O3 = 0 below LQL	68	32	0	0	0
No O3	0	83	17	0	0

Table 2.5. Comparison of leading S(IV) oxidation pathways at the Candelabra Tower, considering ozone to be absent when below the LQL and throughout the entire event.

Sensitivity Conditions	% O_3	% H_2O_2	% O_2 / Fe(III)+Mn(II)	% O_3 and H_2O_2 *	% H_2O_2 and O_2 *
Original	100	0	0	0	0
O3 = 0 below LQL	100	0	0	0	0
No O3	0	100	0	0	0

2.4 Complexation of S(IV) by Formaldehyde

A process that can compete with the oxidation of S(IV) to S(VI) is the complexation of S(IV) with formaldehyde (Boyce and Hoffmann, 1984, Olson and Hoffmann, 1986, 1989, and Kok et al., 1986). This reaction occurs with SO_3^{2-} or HSO_3^- to give hydroxymethanesulfonate (HMS). This has been shown to be important in some fog regimes (Rao and Collett, 1995). For a typical IMS95 value of $[HCHO]_{aq}$ - $[HMS]_{aq}$ of about 33 μM, predicted (assuming gas-liquid equilibrium) gas phase concentrations of HCHO are about 1.7 ppb. This is comparable or higher than the SO_2 concentrations measured at the same time. Therefore, since HCHO is more soluble than SO_2, it is possible that aldehyde complexation could be a significant limiting factor to S(IV) oxidation. Two possible limiting steps of the complexation reaction are the dehydration

of the gem-diol of formaldehyde (methylene glycol) and the bimolecular addition of sulfite and formaldehyde (Olson and Hoffmann, 1986). The bimolecular addition of bisulfite and formaldehyde is much slower than the reaction with sulfite and therefore is not considered further here. The pH dependence of these rates for typical SJV conditions are shown in Figure 2.11 along with the three S(IV) oxidation rates. Since most formaldehyde in the aqueous phase exists as its gem-diol, the rate of the dehydration of formaldehyde could limit HMS formation if HCHO is not absorbed from the gas phase fast enough. At lower pH, dehydration is much faster than the bimolecular addition of SO_3^{2-} and HCHO. Figures 2.12-14 show the rates of S(IV) depletion for each of these steps, along with previously shown S(IV) oxidation rates for the first two fog events at

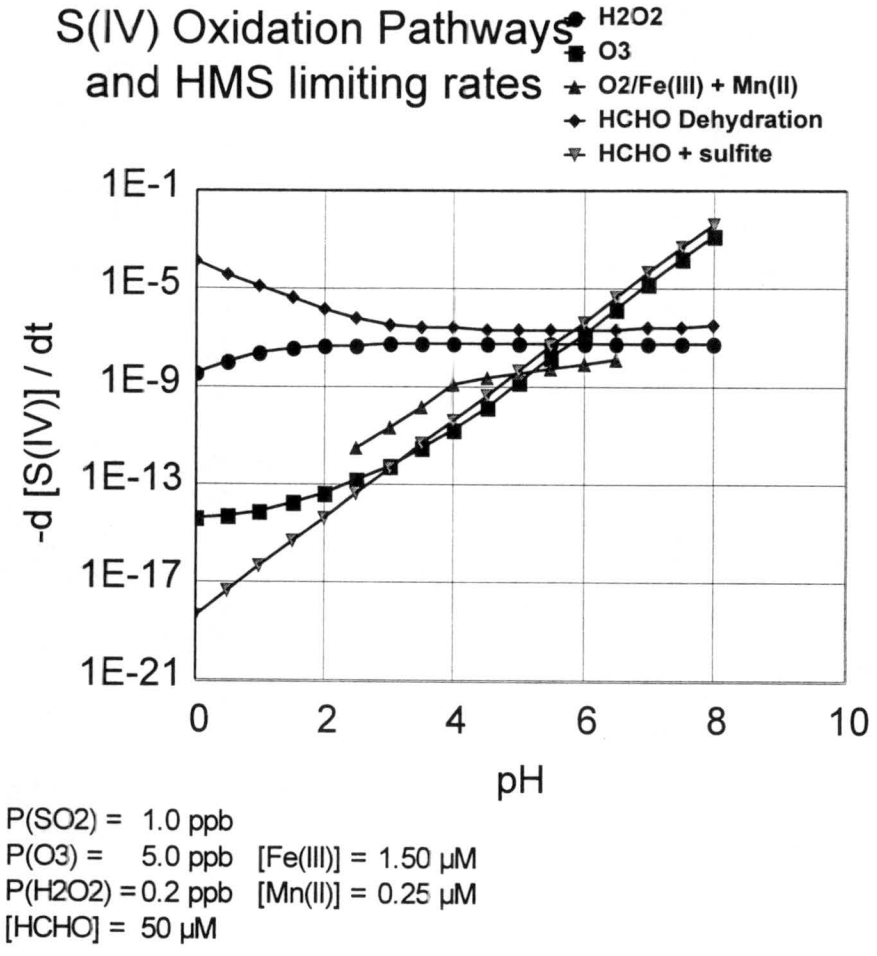

Figure 2.11. HMS formation limiting rates plotted with S(IV) oxidation rates as a function of pH. Rates are given in **M** s^{-1}. Rates are plotted for typical IMS95 fog conditions.

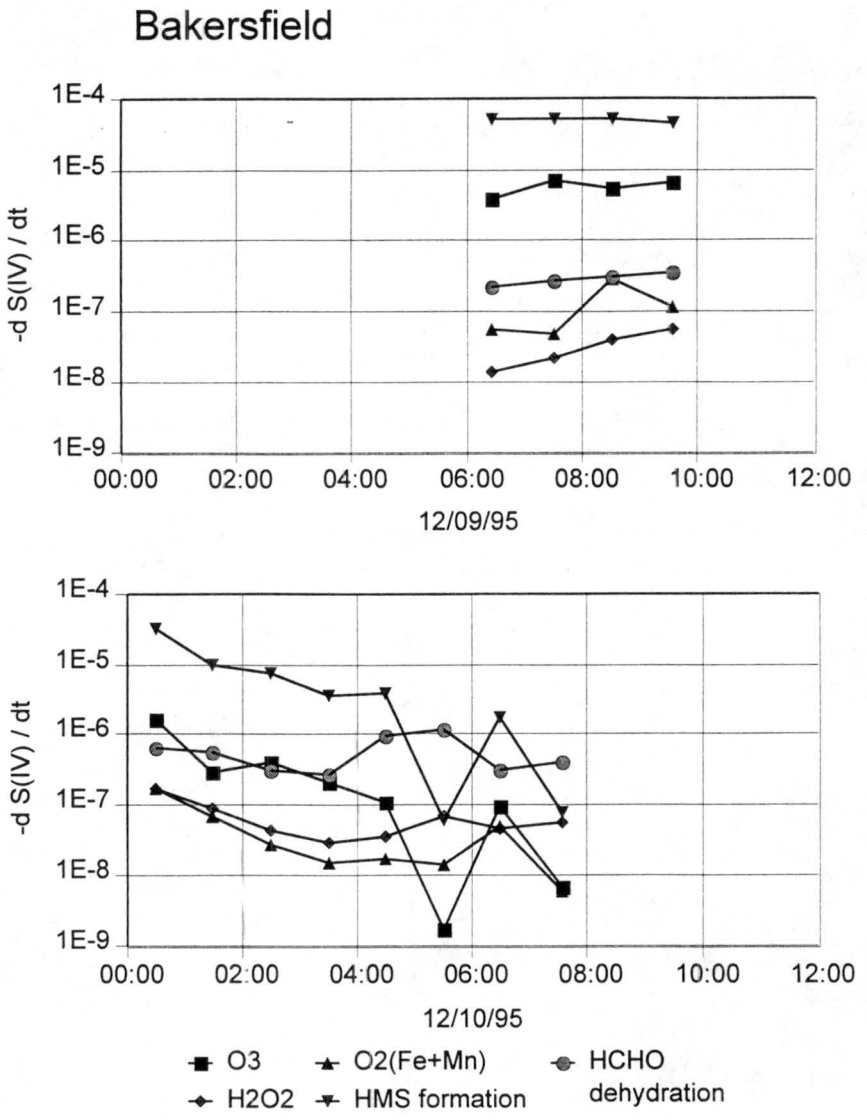

Figure 2.12. Rates for the bimolecular addition of HCHO and SO_3^{2-} (HMS formation) and the dehydration of hydrated HCHO plotted with S(IV) oxidation rates as functions of time for the first two fog events at Bakersfield. Rates are given in **M** s^{-1}.

Bakersfield, Fresno and Kern, calculated for measured aqueous HCHO concentrations. In most cases, the HMS formation reaction is faster than S(IV) oxidation. When insufficient HCHO is available in the gas phase, or if its absorption into the droplets is mass transfer limited, then the dehydration reaction would limit the rate of HMS formation in most cases. If this is the case, then oxidation of S(IV) is still the dominant process during the first event at Bakersfield and during all the events at Kern. The second event at Bakersfield and both events at Fresno exhibit a mixture of S(IV)

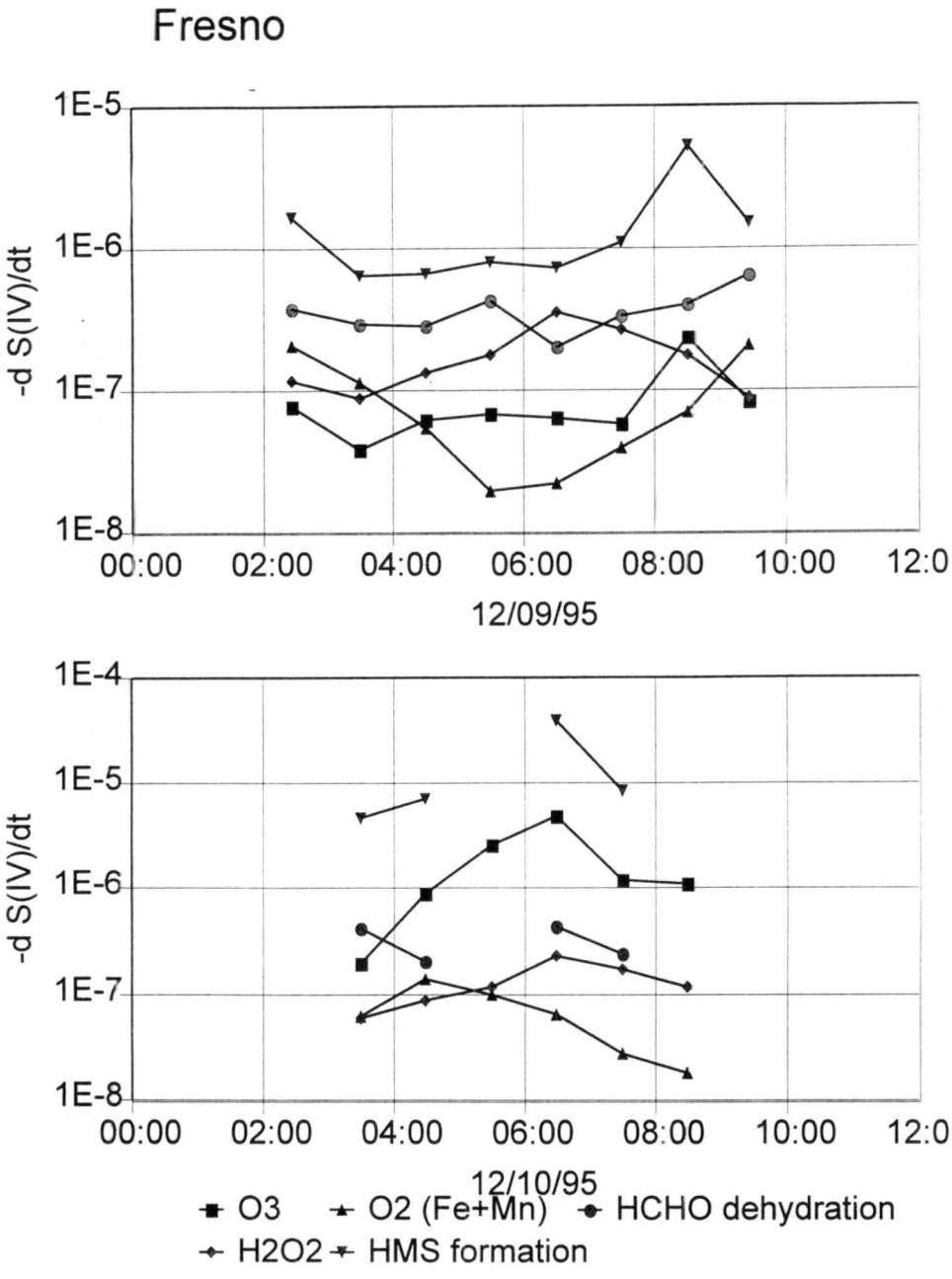

Figure 2.13. Rates for the bimolecular addition of HCHO and SO_3^{2-} (HMS formation) and the dehydration of hydrated HCHO plotted with S(IV) oxidation rates as functions of time for the first two fog events at Fresno. Rates are given in **M** s^{-1}.

oxidation and complexation. It is clear that S(IV) complexation with formaldehyde, therefore, could be an important competitor for available S(IV) in the fog drops but more information is needed about gas and aqueous phase formaldehyde concentrations to be

able to determine how this complexation is limited. Measured HMS concentrations in IMS95 fog samples account for most of the measured S(IV) in many cases, indicating that HMS formation is an important process occurring in the fog. However, this complexation could compete with oxidation for S(IV) only if dissolved SO_2 concentrations cannot be kept at equilibrium levels due to slow mass transport. This is most likely for large drops, or if SO_2 is depleted from the gas phase.

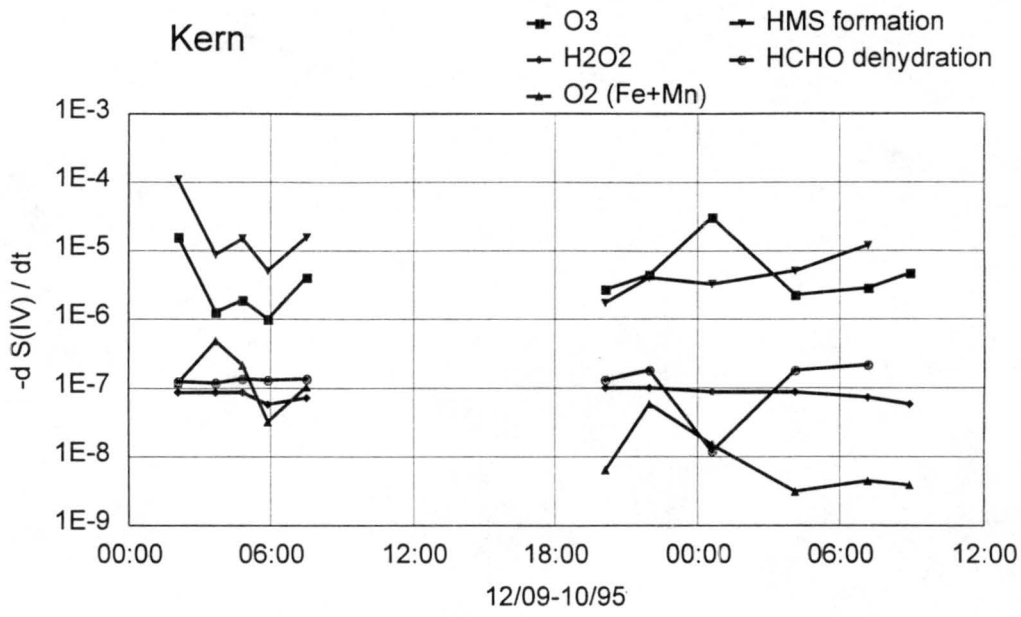

Figure 2.14. Rates for the bimolecular addition of HCHO and SO_3^{2-} (HMS formation) and the dehydration of hydrated HCHO plotted with S(IV) oxidation rates as functions of time for the first two fog events at Kern wildlife Refuge. Rates are given in **M** s^{-1}.

2.5 Effects of Heterogeneity Among Fog Drop Compositions on S(IV) Oxidation

Fog drop composition, including pH, was observed to vary with drop size in events studied during IMS95. For oxidation pathways exhibiting rates which are nonlinear functions of the hydrogen ion concentration, use of the average drop pH can lead to inaccurate predictions of the average sulfate production rate in the fog. This means that calculations based on bulk measurements could yield results much different than what actually occurs in the fog, where chemically distinct drops exist. Chemical heterogeneity as a function of drop size does not alter S(IV) oxidation rates by hydrogen peroxide, since the rate is pH independent over a wide range and H_2O_2 concentrations do not exhibit a strong drop size dependence. For the ozone pathway, which depends nonlinearly on the hydrogen ion concentration, however, variations in acidity as a function of drop size tend to enhance sulfate production. The effect chemical heterogeneity has on the metal-catalyzed oxidation pathway is more difficult to predict since variations in both the acidity and metals concentrations in the drops change the sulfate production rate. Size dependent oxidation rate calculations are imperative to accurately determining sulfate production when the peroxide pathway is not dominant. Since the observed pH difference is often large and the ozone pathway is usually dominant for observed IMS95 conditions, size dependent treatment of the oxidation processes is essential.

Size fractionated samples were collected with a size-fractionating Caltech Active Strand Cloudwater Collector (sf-CASCC) at Kern Wildlife Refuge and with ETH cloud impactors at Fresno and Bakersfield. Both samplers collect a large and a small drop fraction over a given sampling period. The large and small drop fractions expressed in terms of drop diameter correspond to $4 < d < 23$ μm and $d > 23$ μm for the sf-CASCC and to $4 < d < 11$ μm and $d > 11$ μm for the ETH impactor as deployed during IMS95.

Calculations of oxidation rates by ozone as a function of drop size were performed in the same manner as for the bulk samples using the pH of large and small drop samples collected at each of the southern SJV sites. Then the masses of these small and large drop fractions were used to calculate a weighted average H^+ concentration. This $[H^+]_{avg}$ was

used to calculate an oxidation rate that simulates the rate calculated from a bulk sample. This simulated bulk rate is analogous to the situation where the fog drop composition is independent of drop size. A weighted average of the small and large drop oxidation rates gives a more accurate picture of the actual oxidation occurring in the fog, since oxidation is occurring in distinct droplets. This depiction is still rather artificial, however, since many more than two compositions are likely present within the fog. The simulated bulk rate and the weighted average rate can be compared to show the extent to which using an average fog drop composition to predict the S(IV) oxidation rate biases the calculated rate of sulfate production in the fog.

2.5.1 S(IV) Oxidation by Ozone

Figures 2.15-17 show the ozone pathway S(IV) oxidation rates for large and small drop fractions, for a weighted average pH (simulated bulk sample), and the liquid water weighted average of the large and small drop oxidation rates for fog samples collected at Bakersfield, Fresno and Kern. Since the pH of the small drops is much lower than the large drops, the ozone oxidation rate is much slower in the small drops. Since the ozone pathway is nonlinear in $[H^+]$ and most of the water is found in the large drop fraction, this average rate is much different than the 'bulk' rate. In fact, the weighted average rates, which are a better depiction of the actual fog characteristics, are very close to the rates for the large drop fraction. Oxidation rate ratios, calculated as the weighted average rate divided by the bulk rate, determine the magnitude of the effect chemical variations have on sulfate production. When the ratio is larger (smaller) than one, sulfur oxidation is faster (slower) in the chemically heterogeneous fog than one would predict from the average fog composition. Figure 2.18 shows the distribution of ozone oxidation rate ratios calculated for events sampled at all three sites. The ratios are highest at Bakersfield and lowest at Kern, but of significant magnitude at all sites. Table 2.6 lists the ranges and median values for the oxidation rate ratios for the ozone pathway for the three southern SJV sites. Although the median ratios are much higher at Bakersfield and Fresno, it is not possible to say whether these differences are due to the different locations or due to the different size cuts employed by the ETH impactor and the sf-CASCC.

The form of the $[H^+]$ nonlinearity in the ozone S(IV) oxidation rate expression causes the oxidation ratio for this pathway to always be greater than one. For the metal catalyzed autooxidation pathway, both the pH and the metals concentrations affect the S(IV) oxidation rate. Thus, even though pH variations across the drop size spectrum enhance S(IV) oxidation rates, the size dependence of the metal catalyst concentrations could act in the opposite direction, making oxidation ratios of less than one possible (Rao and Collett, 1998).

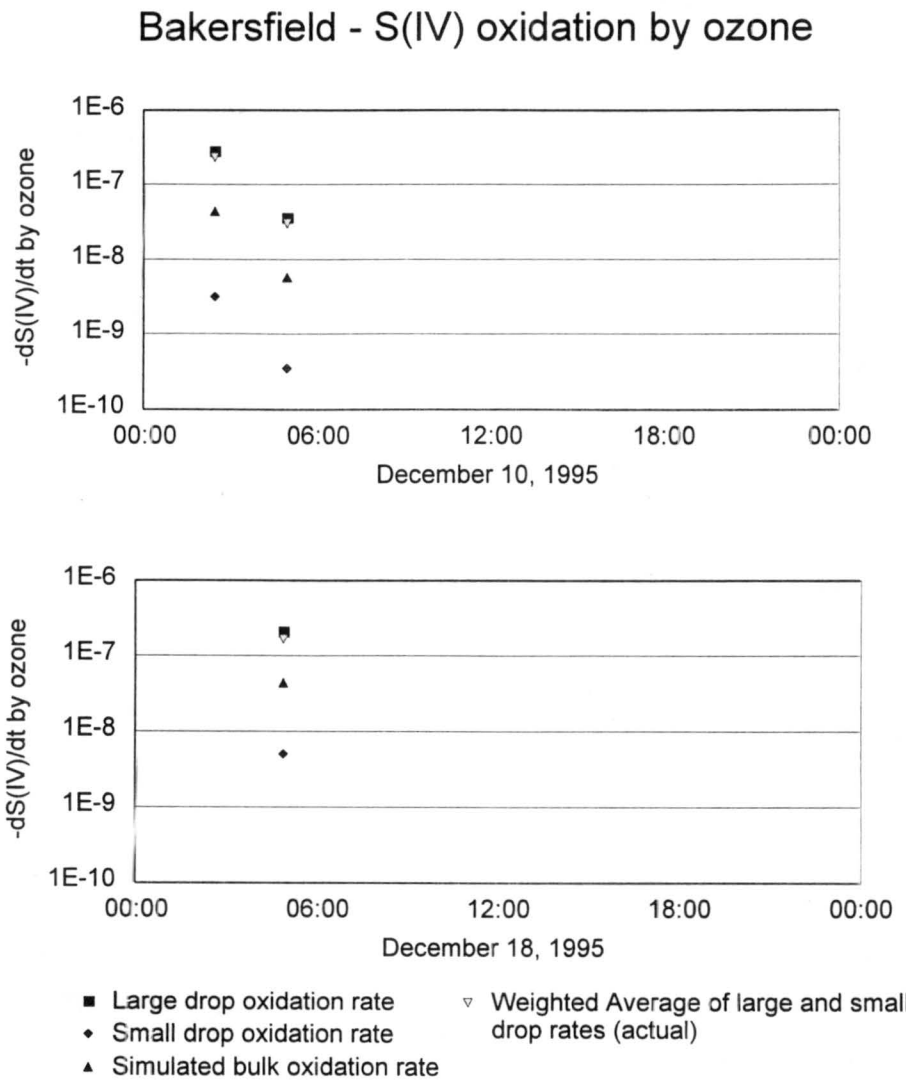

Figure 2.15. The effects of size dependent fog drop acidity on S(IV) oxidation by ozone as functions of time. Large and small drop pH values are from size fractionated samples collected at Bakersfield with an ETH impactor. Simulated bulk rates are calculated from LWC weighted $[H^+]$. Rates are given in **M** s^{-1}.

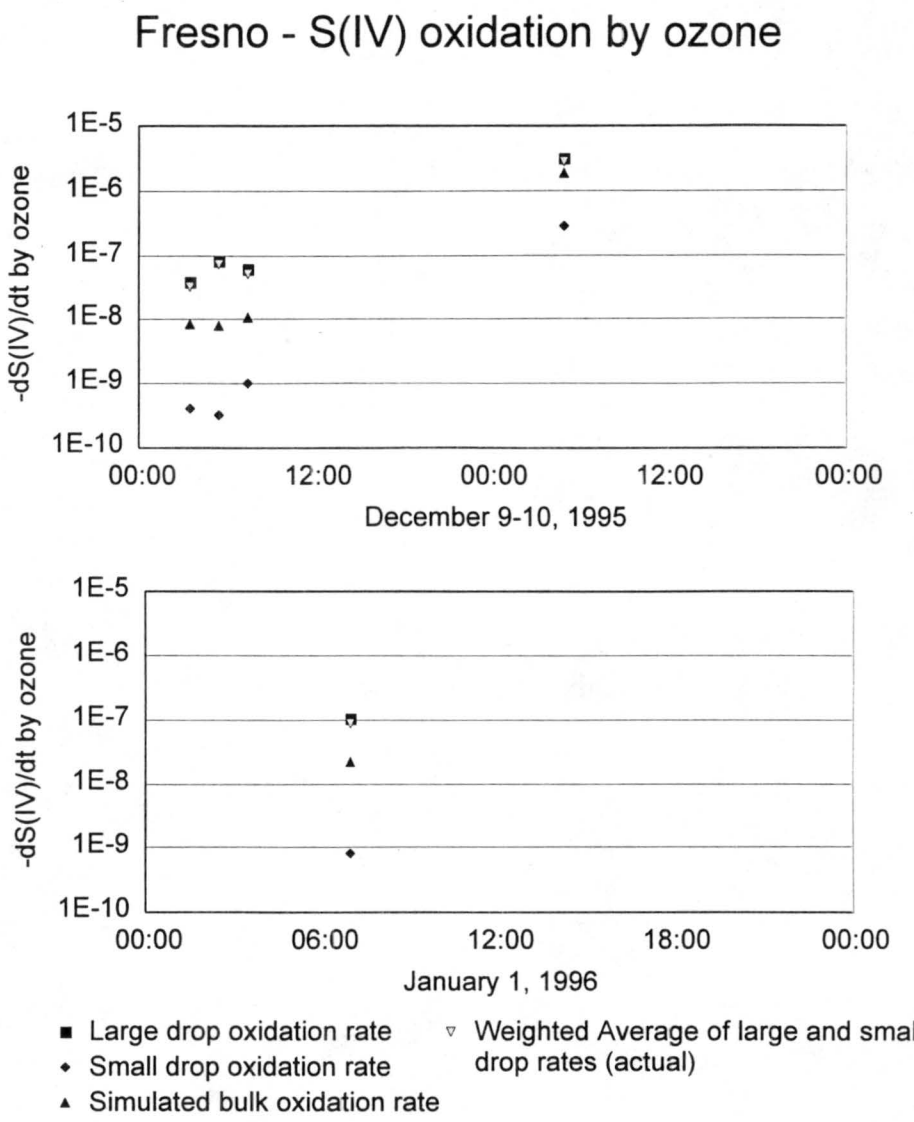

Figure 2.16. The effects of size dependent fog drop acidity on S(IV) oxidation by ozone as functions of time. Large and small drop pH values are from size fractionated samples collected at Fresno with an ETH impactor. Simulated bulk rates are calculated from LWC weighted $[H^+]$. Rates are given in **M** s^{-1}.

2.5.2 Total S(IV) Oxidation

Total oxidation rates for both size fractions and a simulated bulk composition were calculated as the sum of all three oxidation pathways. These rates could be calculated only for Kern samples due to the absence of any size fractionated metals measurements at

Fresno and Bakersfield. Figure 2.19 shows the timelines of the total oxidation rates for the same calculations depicted in Figure 2.17. Figure 2.20 shows the corresponding total oxidation rate ratios for the events sampled at Kern. The ratio ranges from 1.0 to 7.8.

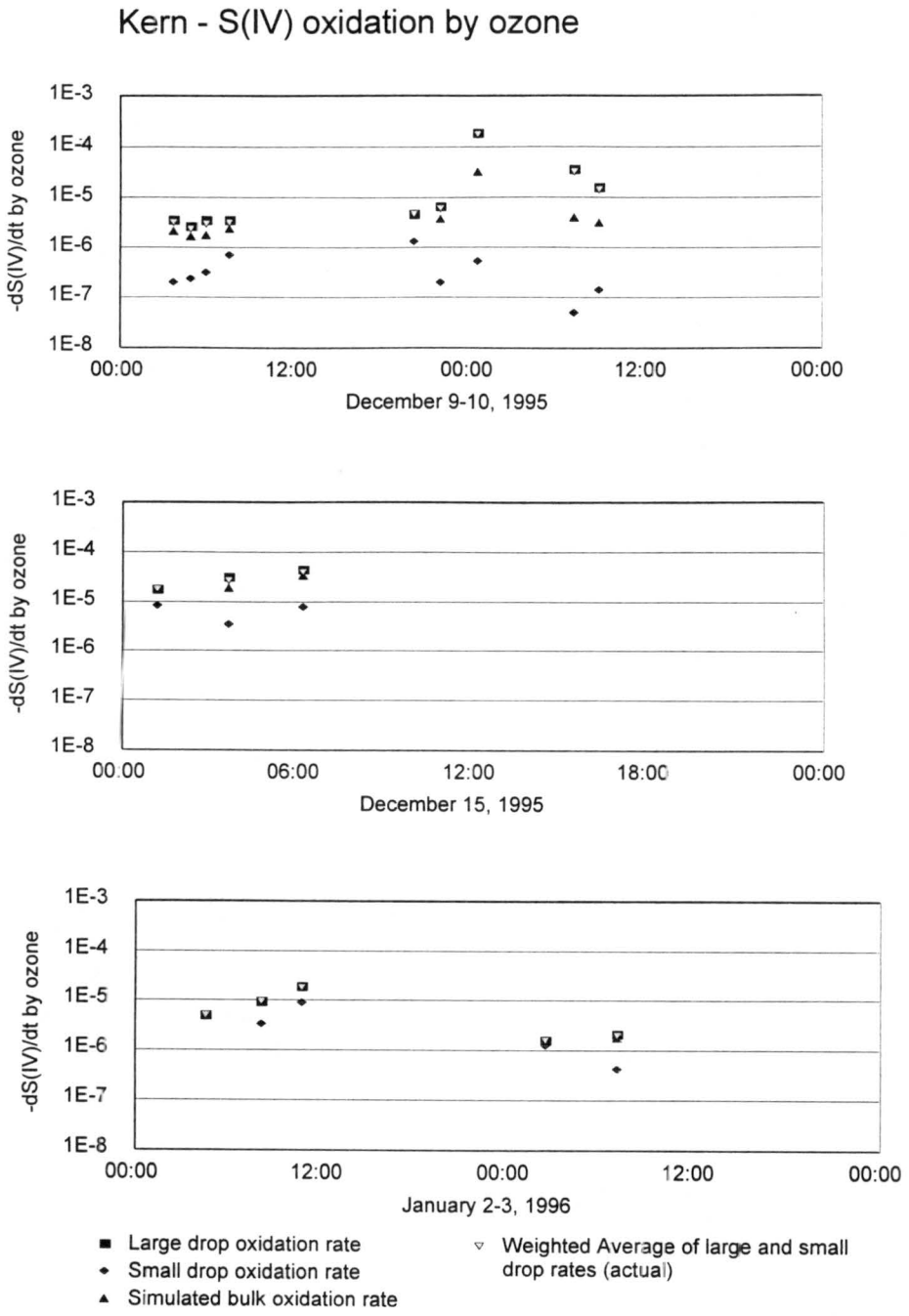

Figure 2.17. The effects of size dependent fog drop acidity on S(IV) oxidation by ozone as functions of time. Large and small drop pH values are from size fractionated samples collected at Kern Wildlife Refuge with the sf-CASCC. Simulated bulk rates are calculated from LWC weighted [H+]. Rates are given in **M** s^{-1}.

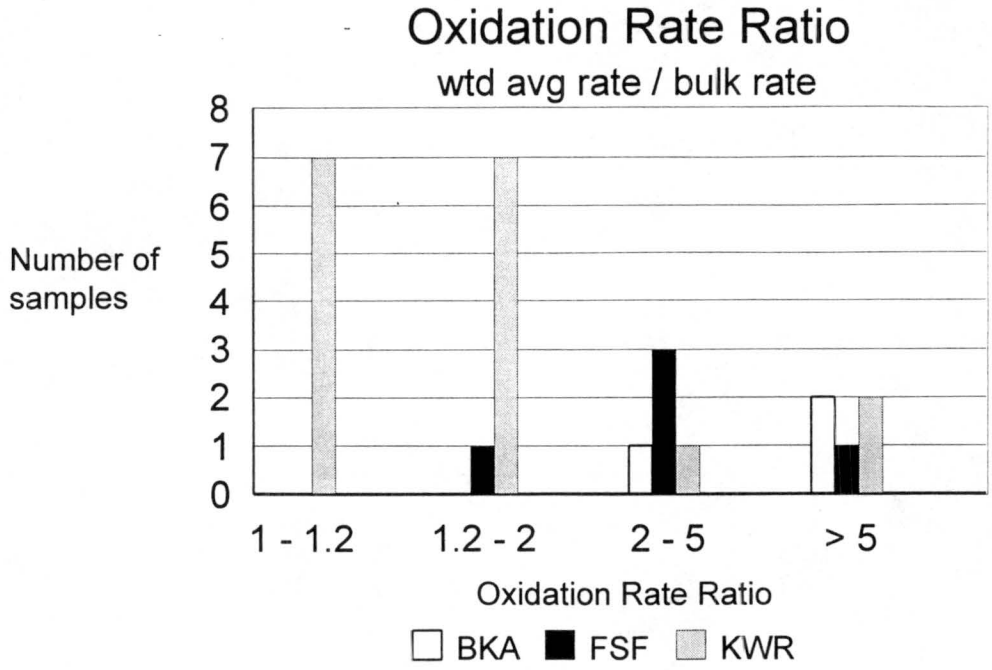

Figure 2.18. Oxidation rate ratios (ratio of the weighted average of large and small drop S(IV) oxidation rates to the simulated bulk rate) for southern SJV samples. Calculated using S(IV) oxidation by ozone only.

Table 2.6. The lowest, highest and median oxidation rate ratios for oxidation by ozone due to variations in fogwater acidity with drop size.

site	# of samples	lowest	highest	median
Bakersfield	3	3.7	5.3	5.2
Fresno	5	1.5	8.9	4.1
Kern	17	1.0	7.9	1.3

The fact that these results are similar to the results for the ozone pathway suggests that the ozone pathway is sufficient to characterize the S(IV) oxidation occurring during these times, since it is significantly faster than the other oxidation rates. Total oxidation rates were calculated for the Fresno and Bakersfield samples for which either the ozone or peroxide path was dominant. When the ozone pathway was dominant, the total oxidation rate ratio was similar to the ratio considering the ozone rate alone. However, for samples

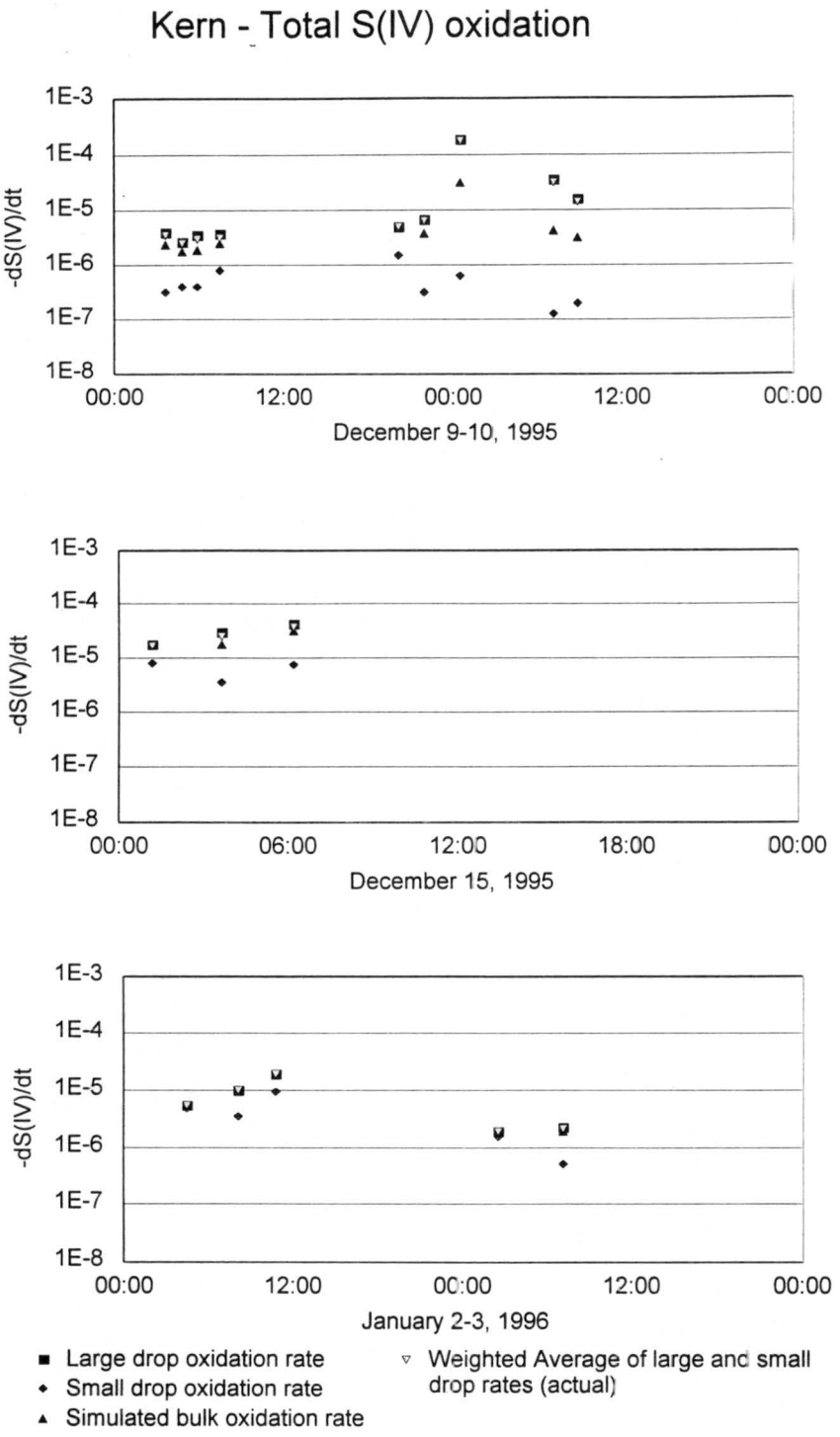

Figure 2.19. The effects of size dependent fog drop acidity on S(IV) oxidation by ozone and metal catalyzed oxygen as functions of time. Large and small drop pH values are from size fractionated samples collected at Kern Wildlife Refuge with the sf-CASCC. Simulated bulk rates are calculated from LWC weighted [H+]. Rates are given in **M** s^{-1}.

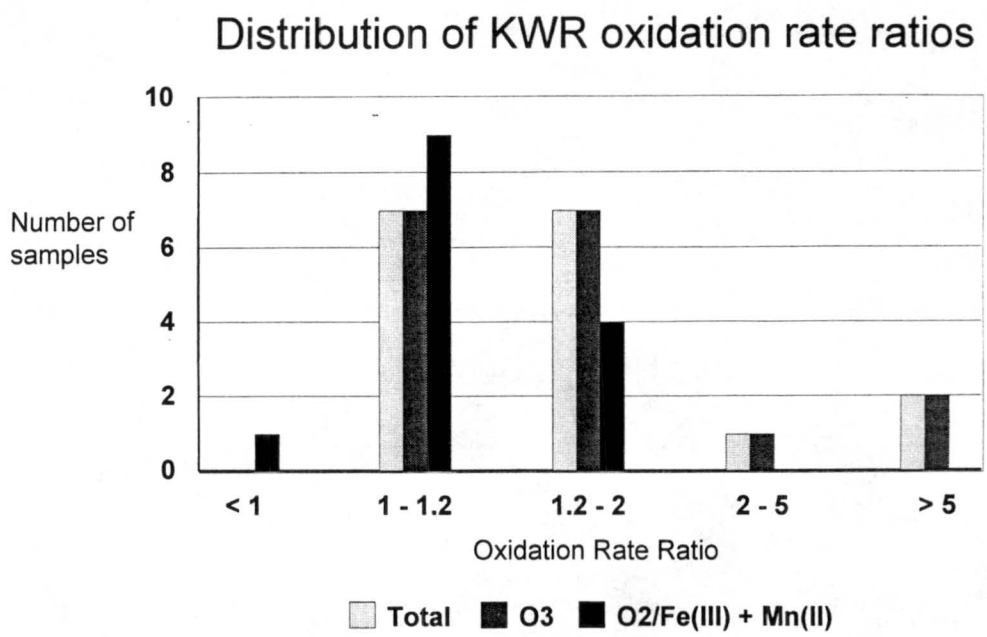

Figure 2.20. Oxidation rate ratios (ratio of the weighted average of large and small drop S(IV) oxidation rates to the simulated bulk rate) for Kern samples. The total oxidation rate ratio is calculated using S(IV) oxidation by all three pathways.

dominated by the peroxide pathway the oxidation rate ratios considering both ozone and peroxide pathways were significantly lower than for just ozone.

The calculated oxidation rate ratios for the IMS95 fog events show that the effect chemical heterogeneity is having on the sulfate production is not negligible and the assumption that the fog drops have a uniform composition spectrum with size is not valid in most cases. Therefore, in these conditions, determining the chemistry using values from bulk collections of fogwater would significantly underestimate the amount of sulfate produced. In fact, these calculations using only two independent compositions still represent a simplified approach to the actual oxidation occurring in the cloud. Resolving the fog drop chemical variations further would be desired, since greater heterogeneity supports even faster S(IV) oxidation rates for the ozone pathway.

2.6 Effects of Heterogeneity Among Fog Drop Compositions on Deposition

Wet deposition to surfaces and the ground is a significant removal process for pollutants and nutrients found in fog drops (Waldman and Hoffmann, 1987). During IMS95 significant deposition of water to the ground was observed. Water from 14.5 cm deposition plates set out at the Fresno site was analyzed for inorganic ions. Table 2.7 shows the plate exposure times, water mass and ion concentrations for water collected on these plates. Fluxes of these species to the surface were estimated using the equation:

$$Ion\ Flux = Flux_{water} \times Ion\ Conc. \qquad (4)$$

where the water flux was calculated from the mass of the deposited water. Fluxes for major ions (nitrate, sulfate and ammonium) ranged from 0.08 to 5.41 nanomoles m^{-2} s^{-1}, showing there was significant removal of these species (see Table 2.8).

Table 2.7. Collection times, water mass (g), and aqueous phase ion concentrations (μN) for the two deposition plate samples collected at Fresno.

Date	Start	End	Mass	Cl^-	NO_3^-	SO_4^{2-}	Na^+	NH_4^+	K^+	Mg^{2+}	Ca^{2+}
12/9	02:17	09:00	3.4	9.8	165	60	10.2	635	10.3	10.4	36.1
12/10	03:00	09:00	1.0	9.3	271	57	6.2	1,185	11.9	5.5	14.0

Table 2.8. Ion fluxes for the two deposition plate samples collected at Fresno. Units are nanomoles/m^2 sec.

Date	Cl^-	NO_3^-	SO_4^{2-}	Na^+	NH_4^+	K^+	Mg^{2+}	Ca^{2+}
12/9	0.08	1.41	0.26	0.09	5.41	0.09	0.04	0.15
12/10	0.03	0.76	0.08	0.02	3.32	0.03	0.01	0.02

Since deposition in a stagnant environment is highly dependent on drop size, knowledge of the drop size-dependent composition of the suspended fog drops is needed to accurately predict the flux of various constituents to the ground. Assuming that sedimentation was the dominant deposition mechanism, calculations were made from size-fractionated fog chemistry observations (sf-CASCC) and measured drop size spectra (PMS-CSASP) to give a calculated flux of each species to the surface. Characteristic drop sizes were obtained from drop size distributions by converting the size distributions

into deposition velocity distributions. Then the average deposition velocity was converted back to a characteristic drop size (one for the whole distribution for a 'bulk' size and one for each part of the distribution sampled by the two stages of the sf-CASCC to give representative small and large drop sizes). Water fluxes for large and small drop fractions were calculated by the equation:

$$Flux = LWC \times X_m \times v_s \tag{5}$$

where LWC is the liquid water content in g m^{-3} (calculated from drop size distributions), X_m is the mass fraction of the water in the small or large size fraction (both of which were calculated from PMS-CSASP size distributions), and v_s is the droplet terminal fall speed given by:

$$v_s = \left[\frac{\varrho_w \, g \, D_o^2}{18 \, \mu}\right] \tag{6}$$

where ρ_w is the density of water, g is the gravitational acceleration, D_O is the characteristic diameter of the large or small fraction derived from the CSASP distributions, and μ is the dynamic viscosity. Ion fluxes were then calculated using the fogwater concentrations from size fractionated samples (C_{lg} and C_{sm}):

$$Ion\ Flux_{\mathrm{lg}\ drops} = Lg\ Drop\ Water\ Flux \times C_{\mathrm{lg}} \tag{7}$$

$$Ion\ Flux_{sm\ drops} = Sm\ Drop\ Water\ Flux \times C_{sm} \tag{8}$$

Estimated errors for these fluxes were calculated assuming the following uncertainties: 20 percent in LWC, 5 percent in mass measurements, 3 μm in characteristic drop size estimates and analytical uncertainties for the ion concentrations as determined in the IMS95 fog study. Figure 2.21 shows the distribution of liquid water between the large and small size drop fractions, derived from measured drop size distributions. Figure 2.22

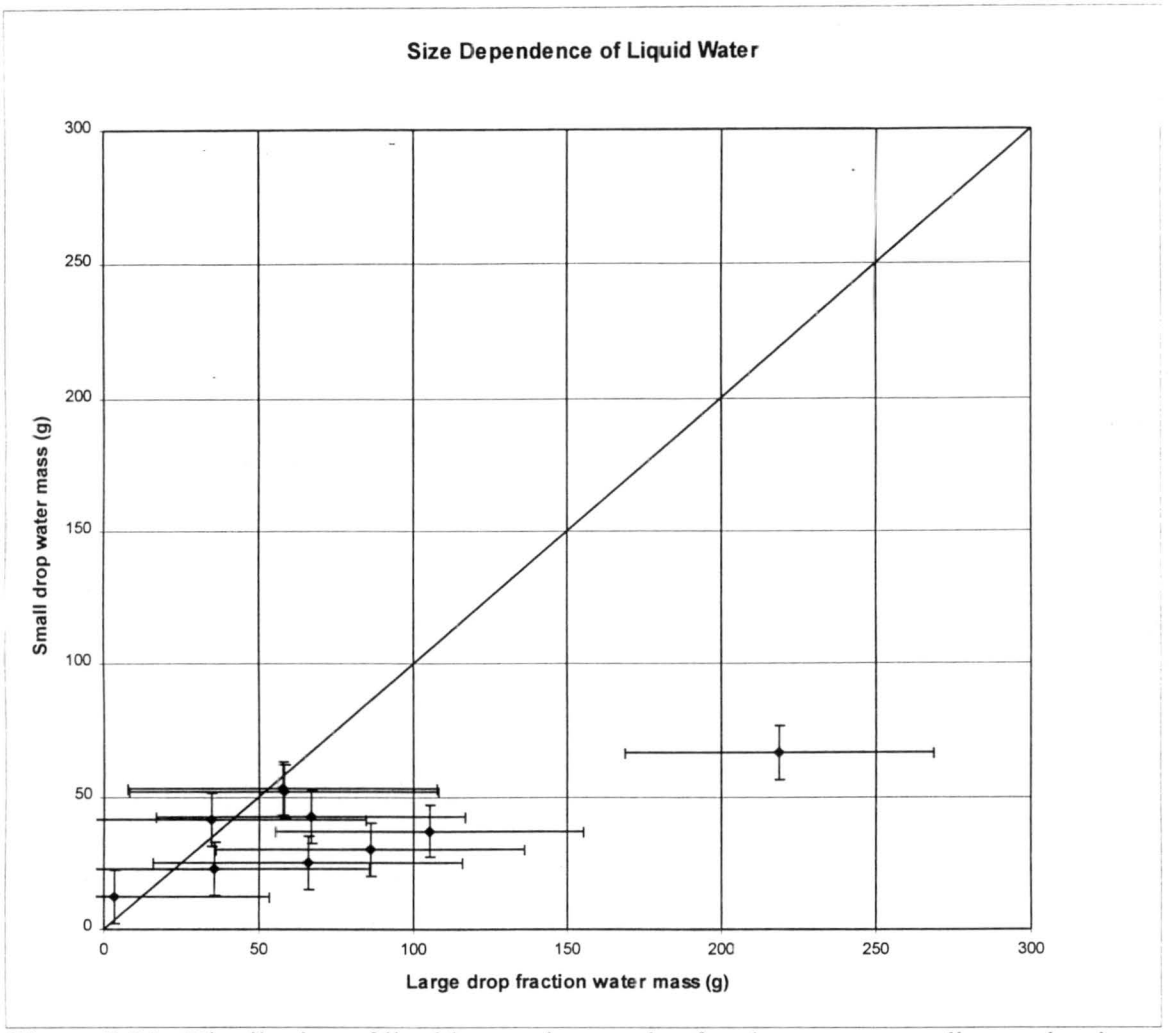

Figure 2.21. Distribution of liquid water in two size fractions corresponding to the size fractionated fog collector size ranges. Calculated from PMS-CSASP data. Error bars represent a 20 percent uncertainty in the liquid water calculations.

shows the small drop fluxes compared to the large drop fluxes for several major ionic species. This figure shows that the large drop ion fluxes are usually less than the small drop ion fluxes, with some scatter. This occurs because the concentrations of the ionic species are much greater in the small drops than in the large drops, but the faster settling velocity of the large drops can occasionally compensate for the concentration difference. The results were compared to similar calculations for a characteristic bulk drop size and a liquid water weighted average of the large and small drop ion concentrations to estimate the magnitude of the effect drop size-dependent chemistry has on prediction of the removal rates of atmospheric species present in the fogwater. Figure 2.23 shows the comparison of the sum of the large and small drop fluxes to the simulated bulk flux for

several major ions. Since the concentrations of the ionic species are significantly more concentrated in small drops that are more slowly removed by settling ($v_s \sim d^2$), the

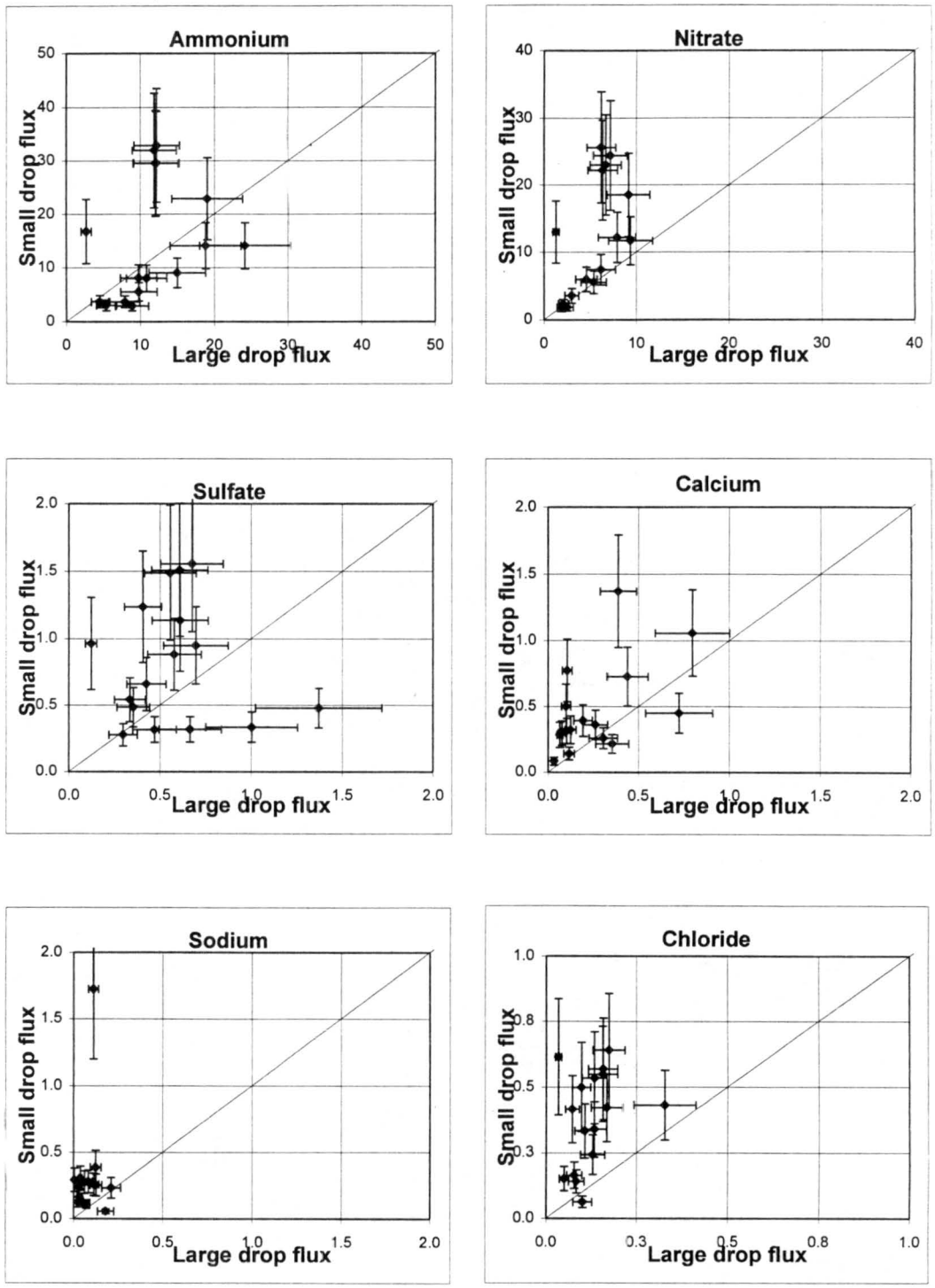

Figure 2.22. A comparison of the large and small drop fluxes of major ionic species. All values are in nanomoles m^{-2} s^{-1}. Error bars represent uncertainties in concentrations, drop sizes and liquid water content, propagated through the flux calculations.

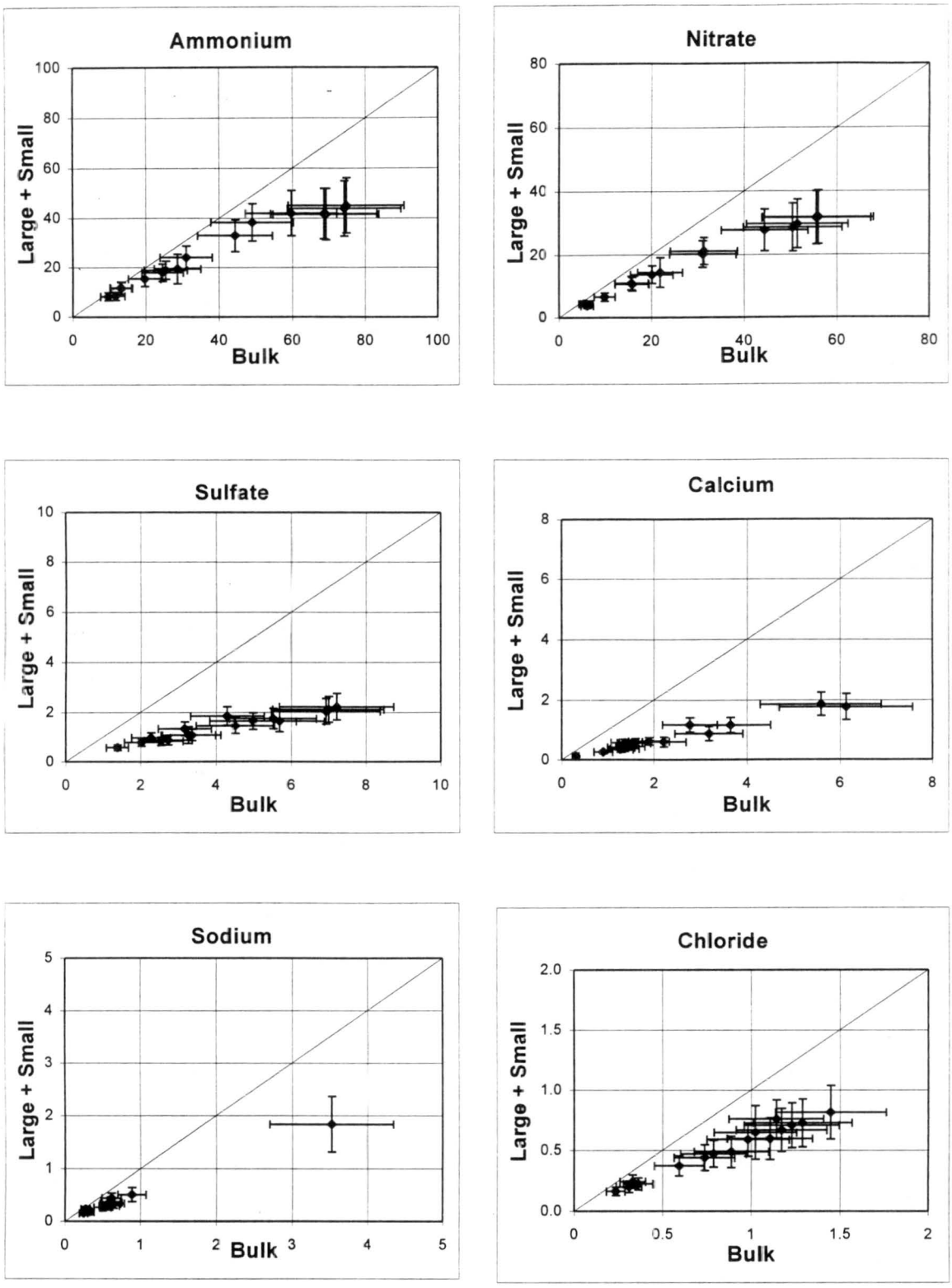

Figure 2.23. A comparison of the sum of the large and small drop fluxes to a flux calculated using simulated bulk fog chemistry. All values are in nanomoles m^{-2} s^{-1}. Error bars represent uncertainties in concentrations, drop sizes and liquid water content, propagated through the flux calculations.

majority of the water being removed is less concentrated than the average fog composition. For the event examined here, estimating the removal of species using bulk fog chemistry and microphysics appears to lead to overprediction of the removal rates of these ionic species by factors as large as 3.5.

In other fog events, some species have been more concentrated in the large drop fraction (Bator and Collett, 1997). Considering only bulk chemistry in such cases would lead to underpredicting the removal rates of these species, since the large drops are settling out faster than average. More concurrent observations of fog microphysics and size-fractionated drop chemistry are needed to accurately characterize the magnitude of the removal of fogwater constituents through wet deposition. By increasing the drop size resolution of the fog chemistry measurements, or by accurately modeling the drop size-dependent chemistry, it should be possible to better predict accurate fluxes of individual solutes to the surface via droplet sedimentation. These measurements should also be accompanied by deposition plate measurements to experimentally verify the water and ion fluxes to the surface during the fog events being characterized.

3. Model Simulations

Cass and Shair (1984) reported a correlation between high aerosol sulfate concentrations in the Los Angeles basin and the occurrence of fog episodes, but the quantitative effects of the fogs on the concentration of the major aerosol species are not yet fully understood. Pandis et al. (1990b) and Hegg and Larson (1990) suggested that sulfate produced is not uniformly distributed over the droplet spectrum. These predictions have been supported by the experimental observations of Collett et al. (1994). Therefore it is necessary to investigate not only the effects of fogs on bulk aerosol concentration, but also the possible effects on the aerosol size/composition distribution.

A rigorous theoretical investigation of the smog-fog-smog cycle requires a mathematical model able to describe in detail the thermodynamics and dynamics of multicomponent aerosols, the microphysics of the condensational growth of a droplet distribution, the droplet removal processes, and the gas and aqueous-phase chemical processes occurring in a fog. Such a model enables us to provide answers to several additional questions associated with the urban fog life cycle. These problems include the aerosol scavenging efficiencies of fogs in the San Joaquin Valley, the uncertainties introduced by measuring in bulk a polydisperse fog droplet distribution, the difference in deposition velocities of different ionic species during fog episodes, and expression of the liquid water flux as a function of the liquid water content for fog models that do not include explicit treatment of droplet microphysics.

We begin with a brief description of the mathematical model employed in this study together with a presentation of the representative SJV fog episode that will be simulated. Next, the effects of fogs on aerosol concentration and aerosol size/composition distribution are investigated. The possible problems posed by the differences in chemical composition of fog droplets of different sizes on fog sampling and on calculations of deposition velocities are presented next. Finally, a possible explanation is presented for the reported differences among the deposition velocities of different ionic species.

3.1 Model Description

The mathematical model employed in this study describes gas-phase chemistry, aerosol dynamics and thermodynamics, aqueous-phase chemistry, droplet microphysics, and wet deposition in a closed homogeneous volume of air in which a fog is formed and dissipated. The primary input to the model is the temperature of the system. This model is an extended version of that developed by Pandis et al. (1990a, b).

The fog physics suggests that the fog life cycle should be divided into three simulation periods, namely the conditioning period (relative humidity, RH, rises from the initial value to a threshold value RH_c close to saturation, chosen as 99%), the rapid growth period ($RH>RH_c$), and the dissipation period (RH drops under RH_c).

During the fog conditioning stage the model simulates the gas-phase chemistry and the aerosol size/composition distribution evolution. Both aerosol dynamics and thermodynamics are considered (Pilinis and Seinfeld, 1987; 1988) and for computational purposes the continuous aerosol size distribution is discretized into *n* uniform sections (Warren and Seinfeld, 1985). The detailed SAPRC gas-phase chemical reaction mechanism (Carter et al., 1986) with the modifications and extensions of Carter and Atkinson (1988) is used for the calculation of the gas-phase reaction rates. This mechanism describes the complex chemical reactions of hydrocarbon/NO_x/SO_2 mixtures in a polluted atmosphere, using 154 reactions and 62 species.

When the relative humidity of the system exceeds the threshold value RH_c, processes described by the model include gas-phase chemistry, aqueous-phase chemistry, microphysics of aerosol and droplets, and deposition. The droplet size distribution is discretized as before into *n* individual size sections but because of the magnitude of the size changes occurring each droplet size section is now allowed to move in the time-diameter space increasing its diameter when water condensation is taking place and decreasing its size in case of evaporation.

The change of the mass concentration of species i in droplet size section l, q_{il}, is calculated by:

$$\frac{dq_{il}}{dt} = \left[\frac{\partial q_{il}}{\partial t}\right]_{cond/evap} + R_{il}^{a}(q_{1l}, q_{2l}, \ldots, q_{nl}) - \frac{v_l}{H} q_{il} \qquad (9)$$

where $[\partial q_{il} / \partial t]_{cond/evap}$ is the mass transfer rate of species i from the gas phase to the aqueous droplets in moving section l, R_{il}^{a} is the rate of change of species i in section l due to aqueous-phase reactions, v_l is the deposition velocity of droplets in section l and H is the fog height. For the water mass transfer rate, the detailed growth equation derived by Pruppacher and Klett (1980) is used and for the remainder of the volatile species, the expression used by Pandis and Seinfeld (1989a) is applied. The use of the detailed growth equation for the multicomponent aqueous solution droplets enables us to describe the activation process exactly without the use of any further assumptions (Pruppacher and Klett, 1980). The reaction rates R_{il}^{a} are derived from the aqueous-phase chemical mechanism presented by Pandis and Seinfeld (1989a) which includes 49 individual aqueous-phase species, 17 aqueous-phase ionic equilibria and 109 aqueous-phase reactions. Field studies in fogs (Dollard and Unsworth, 1983) have indicated that for wind speeds less than 2 m s^{-1}, that are typical of radiation fogs, droplet sedimentation accounts for most of the droplet flux to the ground. Therefore, the deposition velocity of fog droplets is approximated by Stokes law as long as the diameter of the droplets remains less than 50 μm.

Droplet coagulation is neglected and the number concentration of droplets in each section l, N_l, changes only due to droplet deposition and is described by

$$\frac{dN_l}{dt} = -\frac{v_l}{H} N_l \qquad (10)$$

The change in section diameter, D_l, is calculated by

$$\frac{dD_l}{dt} = \frac{2}{N_l \rho_l D_l^2} \sum_{i=1}^{Nv} \left[\frac{\partial q_{il}}{\partial t}\right]_{cond/evap} \qquad (11)$$

where ρ_l is the density of droplets in section l, and N_v is the number of volatile species. The turbulence induced by the radiative cooling of the fog top and the entrainment of air in the fog layer have been neglected in this study. Lillis et al. (1998) discuss entrainment in IMS95 fogs. They conclude it plays an important role in increasing sulfate production rates and nitrate and ammonium concentrations aloft.

3.2 Evaluation of Fog Model - Episode of December 9-10, 1995

Unfortunately, no complete data set was collected in IMS95 for a full evaluation of the present model. Such a data set should include aerosol size/composition distributions before and after the fog episode, droplet size/composition distributions during the episode and measurements of the fog removal fluxes. We have combined data collected during the fog episode of December 9-10 in SJV from different sites (removal rates from Fresno, aerosol size/composition distributions from Bakersfield, and fog droplet size composition distribution data from Fresno and KWR) for the model evaluation. The initial conditions selected correspond to Fresno.

The model has been applied with 14 logarithmically spaced sections covering initially the diameter range from 0.1 to 10 μm (Figure 3.1). This choice of section number represents a reasonable compromise between computational accuracy and keeping the required computing time at a reasonable level (Gurciullo and Pandis, 1997). Increasing the current number of sections causes an exponential increase in computing time without changing the conclusions reached in the present work. The initial aerosol size/composition distribution shape was based on the measurements in Bakersfield during the same day. This distribution was scaled by the total concentrations measured in Fresno before the fog started. The implicit assumption here is that the aerosol size distributions in Fresno and Bakersfield on December 9 were similar.

The temperature variation during the episode was calculated by the detailed fog dynamics model of Pandis and Seinfeld (1989b) off-line and was used as an input to the present calculation. The simulation starts at midnight at a RH equal to 95%.

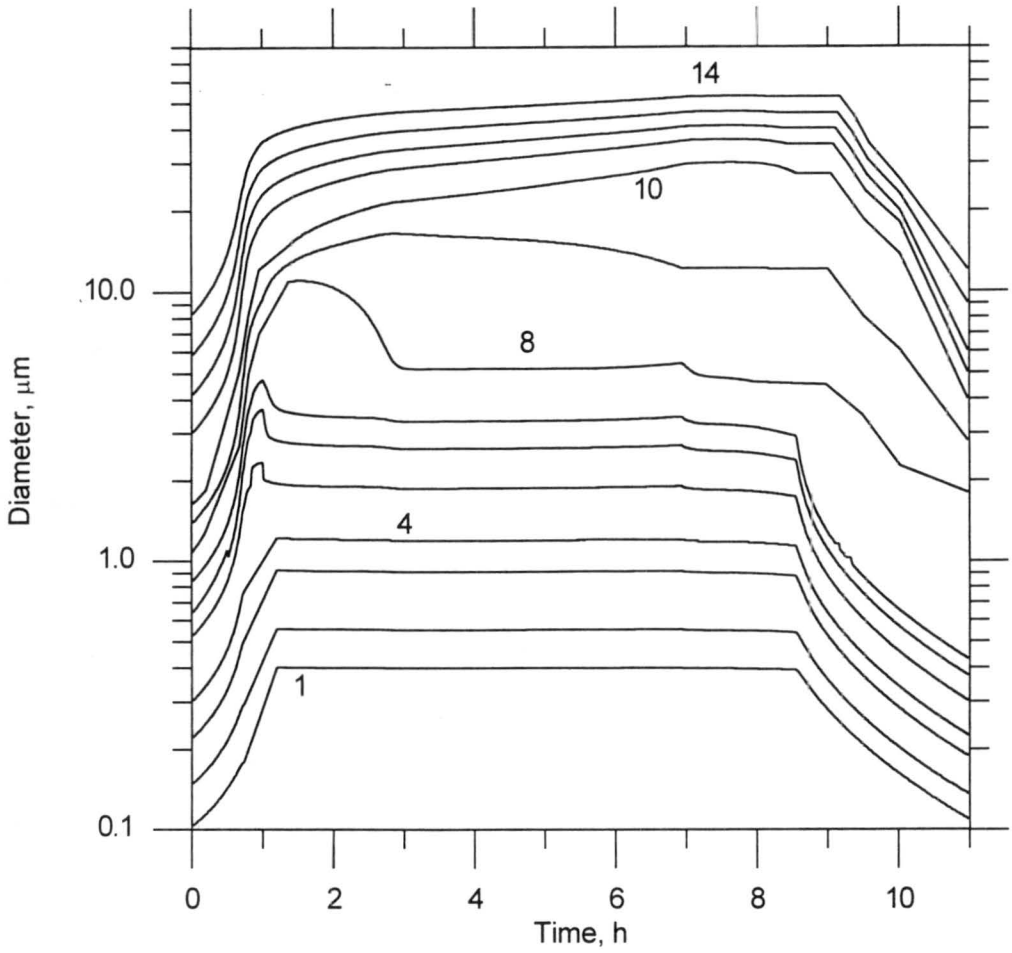

Figure 3.1. Predicted evolution of the diameters of the aerosol/droplet groups during the fog episode.

3.2.1 Fogwater Size Distribution

The evolution of the predicted particle size spectrum is shown in Figure 3.1. All particles grow significantly in size with the 0.1 μm aerosol reaching a diameter equal to 0.3 μm, and the 1.5 μm particles (section 8) becoming as large as 10 μm. The 1.5 μm particles get activated and become fog droplets in the fog development stage (around 2 a.m.) but later on as the supersaturation inside the fog decreases they get deactivated and evaporate. From 3 a.m. to 7 a.m. the fog is stable and the particles in the first 8 sections are in stable equilibrium with their supersaturated environment and their diameters remain approximately constant. The fog is predicted to evaporate at around 9 a.m. and at this time the diameters of all particles decrease rapidly.

The predicted water mass distribution is shown in Figure 3.2. Most of the atmospheric liquid water content is in the fog droplets in the diameter range 10-30 μm. Particles smaller than 3 μm are interstitial aerosol particles with little liquid water (note the logarithmic scale). Droplets larger than 30 μm also contribute little to the liquid water content of the fog because of their rapid removal from the fog layer.

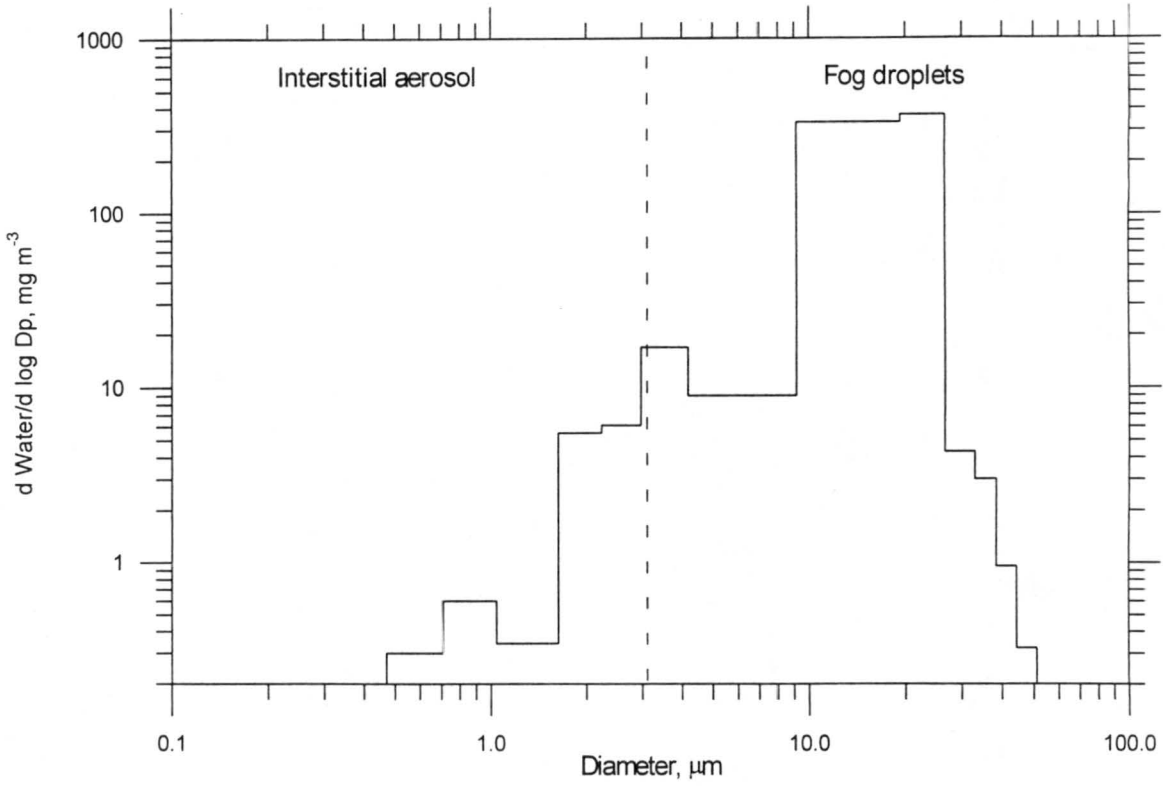

Figure 3.2. Predicted particle water mass distribution at 4 a.m.. Particles smaller than approximately 3 μm are not activated and are characterized as interstitial aerosol. Particles larger than 3 μm are characterized as fog droplets.

Figures 3.1 and 3.2 indicate that the distinction between fog droplets and interstitial aerosol is not as simple as it is often thought. Particles in the size range 3-10 μm have enough liquid water and have grown sufficiently from their original size to be considered droplets. However, their solute concentrations are much higher than the rest of the fog droplets and one could characterize them as interstitial aerosol. The existence of these particles should be considered during the design and interpretation of the results of

fogwater sampling systems. For the purposes of the present study the cutoff between interstitial aerosol and fog droplets will be at around 3 μm (Figure 3.2).

3.2.2 Aerosol Scavenging Efficiency

The aerosol scavenging efficiency of the fog determines the extent to which the fog droplet concentrations are influenced by the preexisting aerosol. This scavenging efficiency depends on the maximum supersaturation reached in the fog and on the preexisting aerosol size composition distribution.

Ten Brink et al. (1987) observed nearly complete scavenging of aerosol sulfate in clouds. Munger et al. (1990) reported aerosol scavenging ratios always lower than 100% and, depending on the method used, ranging from 10% to 90%. In a theoretical study of wet removal of atmospheric pollutants, Jensen and Charlson (1984) calculated that for an average urban aerosol population nucleation scavenging efficiency is close to unity for convective clouds, but for stratiform clouds it decreases rapidly as the updraft velocity is lowered. Flossmann et al. (1985, 1987) reported calculated aerosol scavenging efficiencies equal to or larger than 90% in typical cloud environments.

The scavenging efficiencies for the fog episode under consideration can be calculated from the initial species size distributions. Figure 3.1 indicates that the aerosol in the last 7 sections (sections 8-14) became fog droplets during the fog formation stage. Therefore the aerosol scavenging efficiencies for the various species will be equal to the fraction of the species in particles larger than approximately 1.5 μm in diameter (at 95% RH). This result is consistent with the CMU measurements during IMS95 that suggested that particles smaller than 1 μm (at RH around 100%) were not affected by the fog. The maximum scavenging efficiencies were 81% for sulfate, 76% for nitrate, and 65% for ammonium. These results are consistent with the estimates of Pandis et al. (1990a) for typical urban radiation fogs. Note that because some of the fog droplets get deactivated during the fog lifetime (Figure 3.1) these scavenging efficiencies are reduced to around 55% for sulfate and nitrate and 50% for ammonium during most of the fog lifetime. The

mean scavenging efficiencies for the whole episode are 62% for sulfate, 60% for nitrate, and 53% for ammonium.

Calculation of these efficiencies from measurements is inhibited by the production of sulfate and the transfer of ammonia and nitric acid to the fog droplets during the fog formation stage. The predicted size distributions of sulfate, nitrate, and ammonium during the mature fog stage are shown in Figures 3.3-3.5.

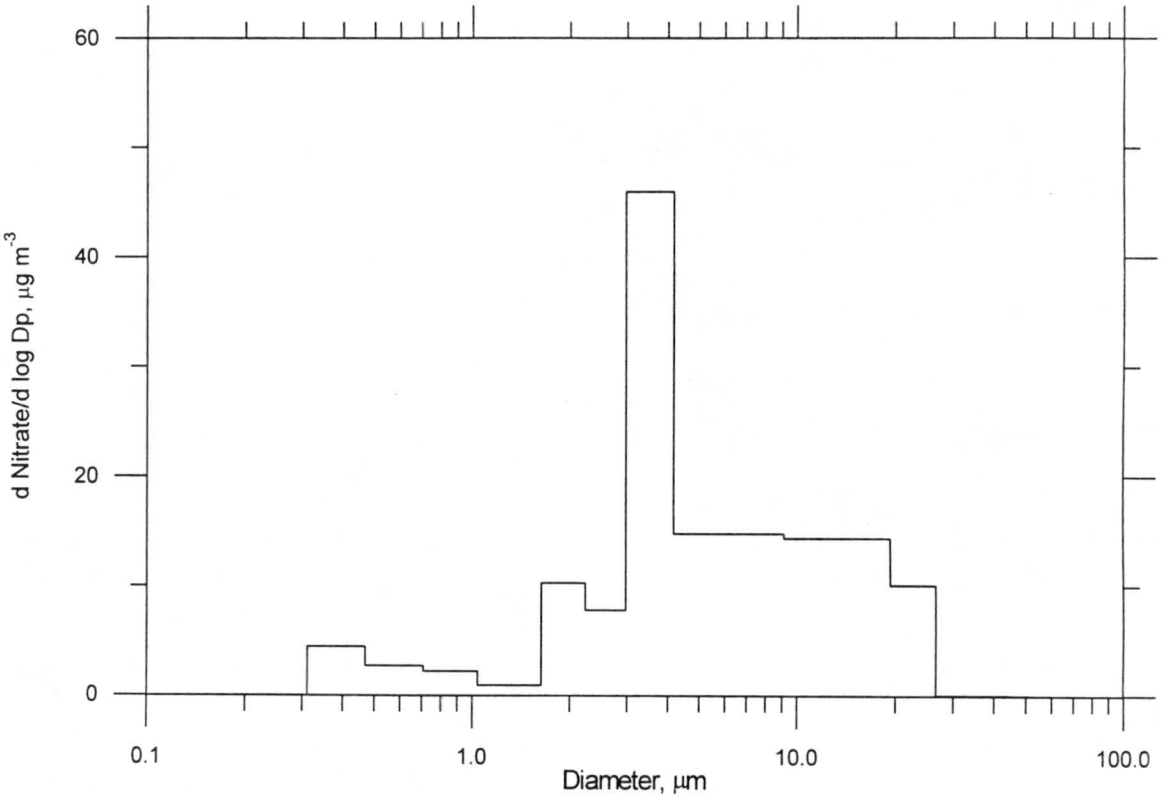

Figure 3.3. Predicted nitrate size distribution at 4 a.m. The distribution includes both interstitial aerosol and fog droplets.

The nitrate size distribution is characterized by a peak at the 3-5 µm size range (Figure 3.3). This nitrate peak is the result of dissolution of gas-phase nitric acid during the fog formation stage and the preexisting ammonium nitrate in these particles.

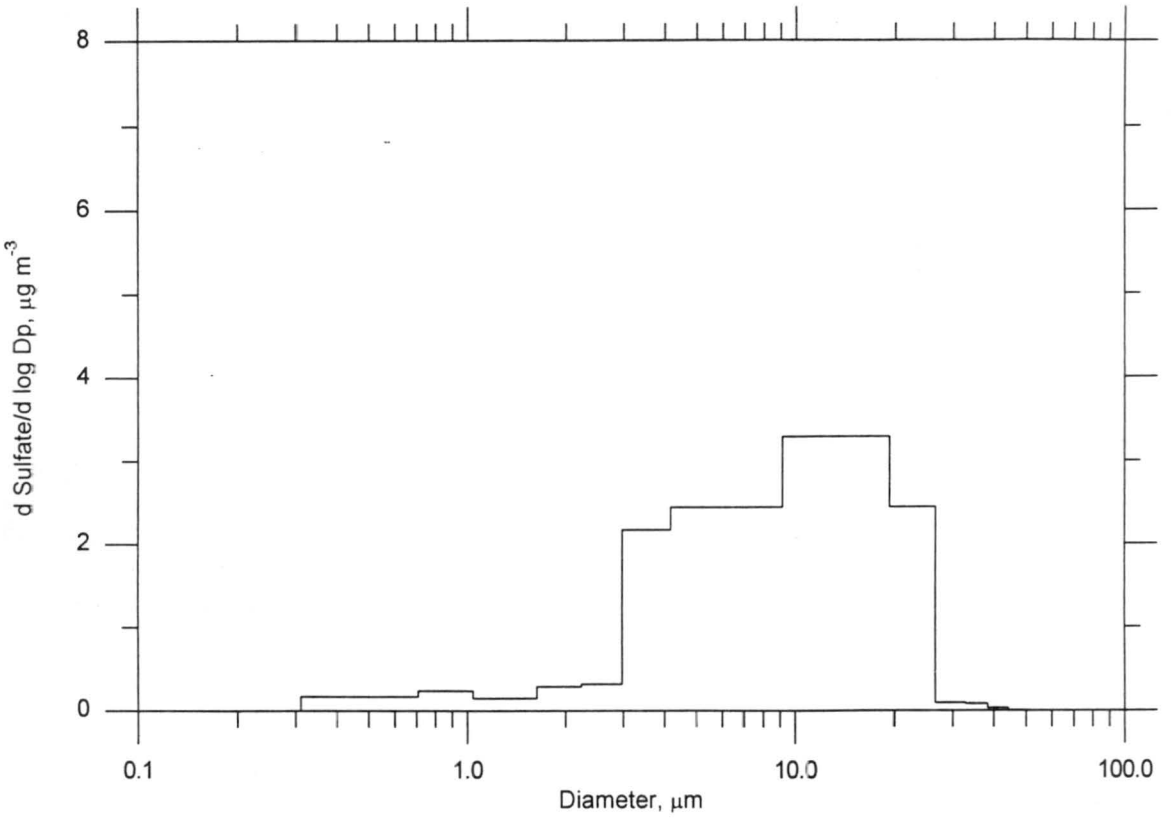

Figure 3.4. Predicted sulfate size distribution at 4 a.m. The distribution includes both interstitial aerosol and fog droplets.

The sulfate size distribution is qualitatively different than that of nitrate. Most of the sulfate is produced in the particles that have most of the liquid water (and not the higher surface area) and as a result the peak of the sulfate distribution is in the 10-20 μm range. The sulfate distribution is rather similar to the liquid water content distribution (Figure 3.2). Finally the ammonium distribution is bimodal (Figure 3.5) with one mode corresponding to the nitrate peak and a second mode accompanying the sulfate mode. This bimodality is the result of the effort of ammonia to neutralize both the nitrate-rich and the sulfate-rich particles.

The transfer of material from the gas phase and the production of sulfate inside the fog droplets result in the existence of the majority of nitrate/sulfate/ammonium in particles larger than 4 μm during the mature fog stage. Estimation of the aerosol scavenging efficiency based on measurements of these distributions would lead to a significant overprediction. For example, Figure 3.3 indicates that 84% of the ambient nitrate at that

moment is in particles larger than 4 μm. However, almost half of the nitrate was in the gas phase before the fog formation and is not the result of nucleation scavenging of the preexisting ammonium nitrate aerosol.

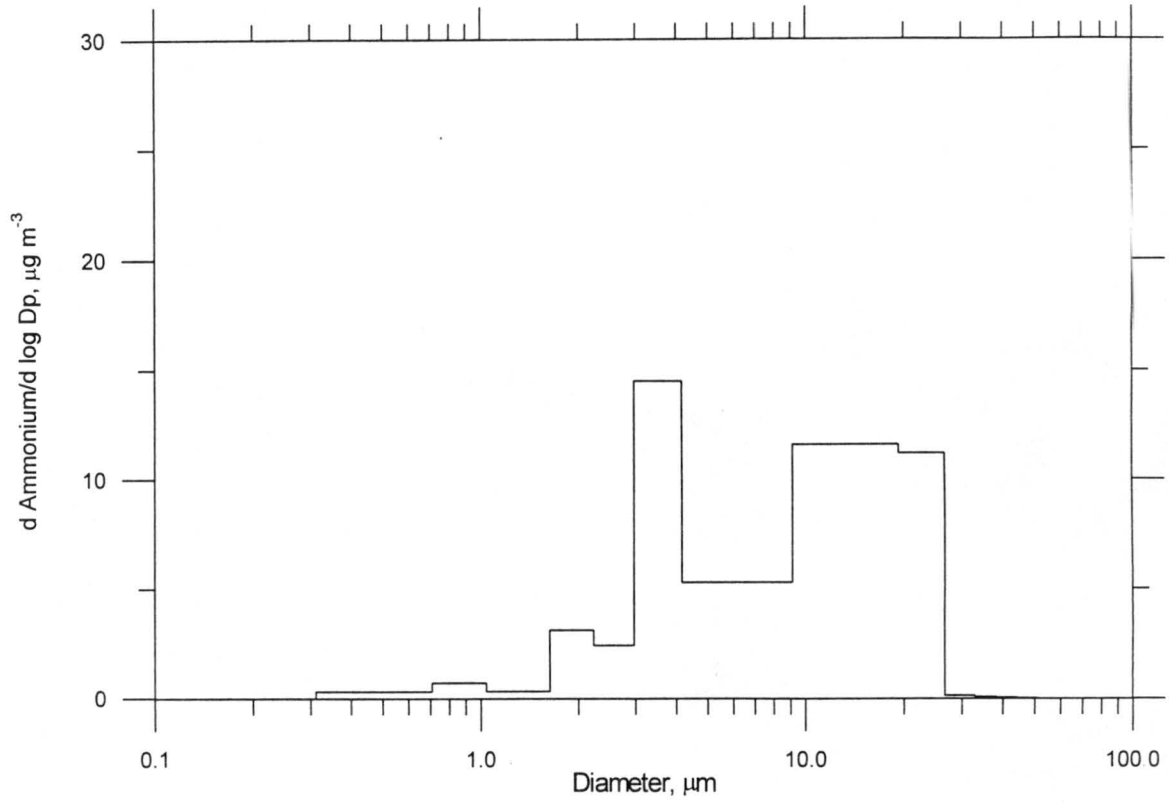

Figure 3.5. Predicted ammonium size distribution at 4 a.m. The distribution includes both interstitial aerosol and fog droplets.

The above estimates of aerosol scavenging efficiencies can be used to improve the assumptions used in fog models like the one developed by Pandis and Seinfeld (1989b). In that model, explicit droplet microphysics is not considered and the initial fogwater concentrations are calculated by assuming that a fraction of the preexisting aerosol is scavenged by the fog droplets.

3.2.3 Aqueous Concentration Distributions

The evolution of the predicted pH distribution is depicted in Figure 3.6. Droplets smaller than 10 μm in diameter have a pH around 6 while the larger droplets are less acidic with pH values in the 6.7-7.0 range. The cause of this pH variation is mainly the presence of

high nitric acid concentrations (resulting from preferential transfer of the gas-phase nitric acid) to these smaller particles during the fog formation stage. The drop size-resolved pH measurements of CSU during this episode are in good agreement with the pH values calculated by the model.

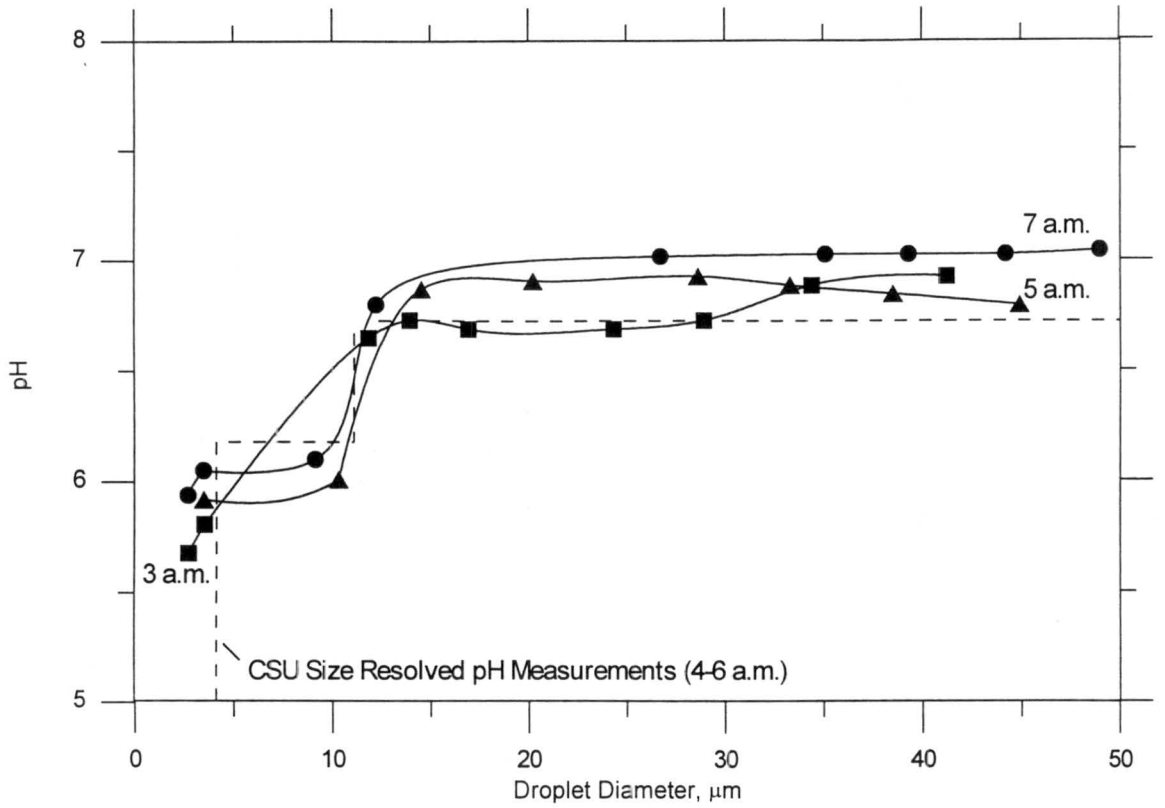

Figure 3.6. Predicted pH size distribution compared against the small ($4 < d < 11$ μm) and large ($d > 11$ μm) drop pH values measured during the episode using an ETH cloud impactor.

The existence of most of the available nitrate (both preexisting ammonium nitrate and dissolved nitric acid vapor) in the 3-15 μm size range results in nitrate concentrations of the order of 1000 μM or higher in these particles. The nitrate aqueous-phase concentrations of larger droplets are predicted to be a factor of five or more smaller (Figure 3.7). At 3 a.m. a peak in the nitrate concentrations for the 17 μm droplets is predicted, but this maximum soon relaxes leading to a monotonically decreasing nitrate aqueous-phase concentration. These concentration differences are in good agreement

with the size-resolved drop chemistry measurements in KWR (only pH size dependence was measured at Fresno) indicating that the present model is able to reproduce well the main features of the dependence of the droplet solute concentration on their size.

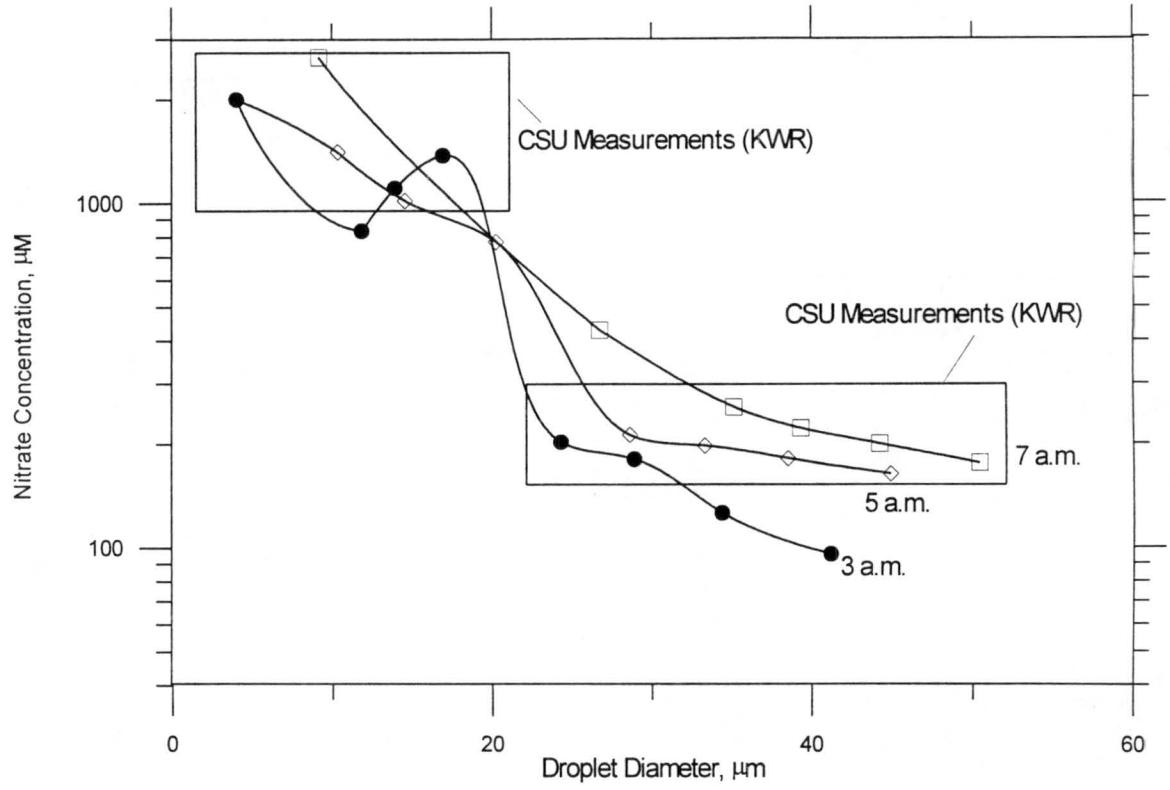

Figure 3.7. Predicted nitrate concentration distribution at 3, 5 and 7 a.m. during the Fresno fog episode. Also shown is the range of the CSU measurements in Kern Wildlife Refuge for the same episode.

The measured bulk sulfate concentrations are compared against the predicted concentrations of small (4-23 μm in diameter) and large (>23 μm) fog drops in Figure 8. The model predicts that the small droplets after the fog formation stage have sulfate concentrations that are as much as an order of magnitude higher than the larger ones. This result is in agreement with the sulfate concentration dependence measured in Kern. The predicted concentration evolution is the combined result of droplet growth and evaporation, sulfate production, and growth of small droplets to larger ones. The sulfate

production is taking place preferentially in the smaller droplets leading to the higher sulfate concentrations.

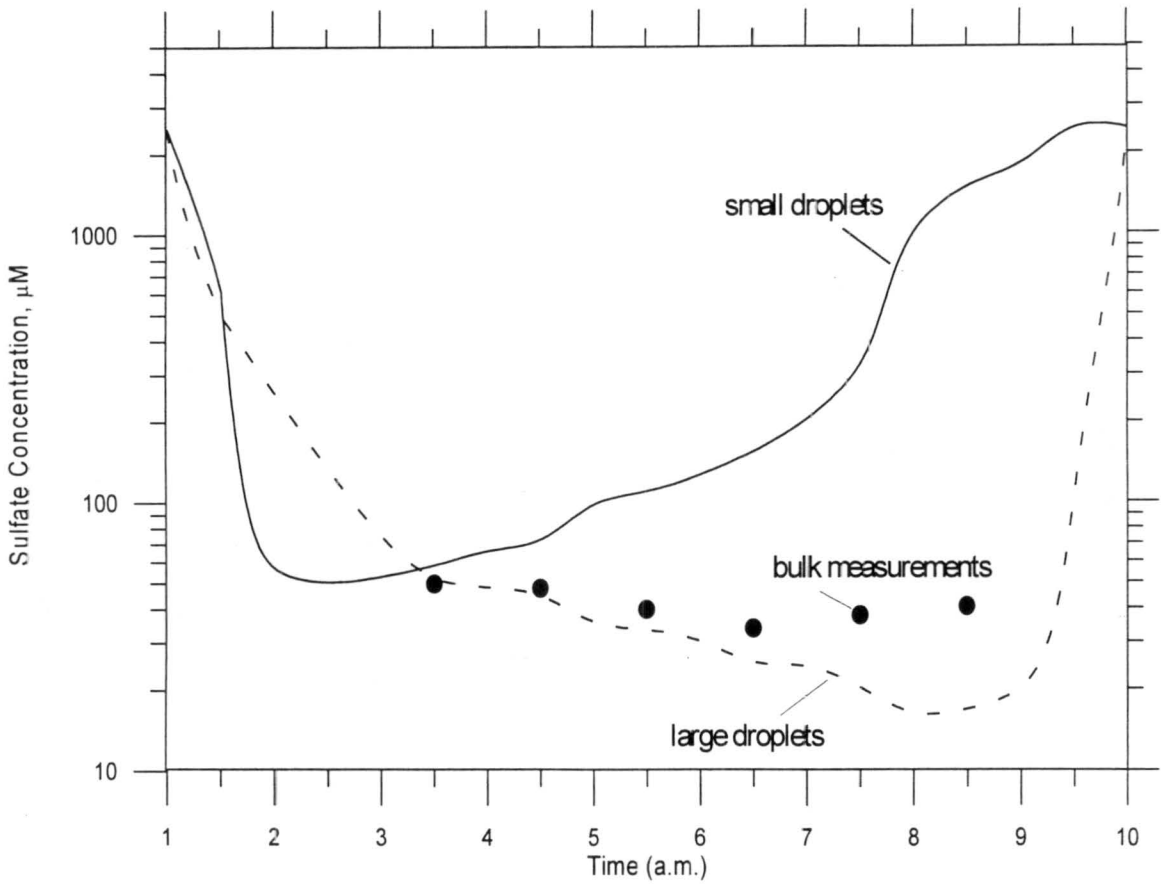

Figure 3.8. Predicted sulfate aqueous-phase concentrations for small ($4 < D_p < 23$ μm) and large (Dp > 23 μm) fog droplets as a function of time. Also shown are the bulk sulfate measurements for the same episode.

3.2.4 Effects of fog on aerosol concentration

The evolution of the particulate concentrations of the major inorganic aerosol species is shown in Figure 3.9. At 1 a.m., at the beginning of the fog episode, there are 14.1 μg m^{-3} of nitrate, 1.45 μg m^{-3} of sulfate, and 7.1 μg m^{-3} of ammonium in the particulate phase. During the next hour the ambient relative humidity increases from 95 to 100% and the fog formation starts. The aerosol liquid content increases during this conditioning period shifting the equilibrium of ammonia and nitric acid towards the aerosol phase.

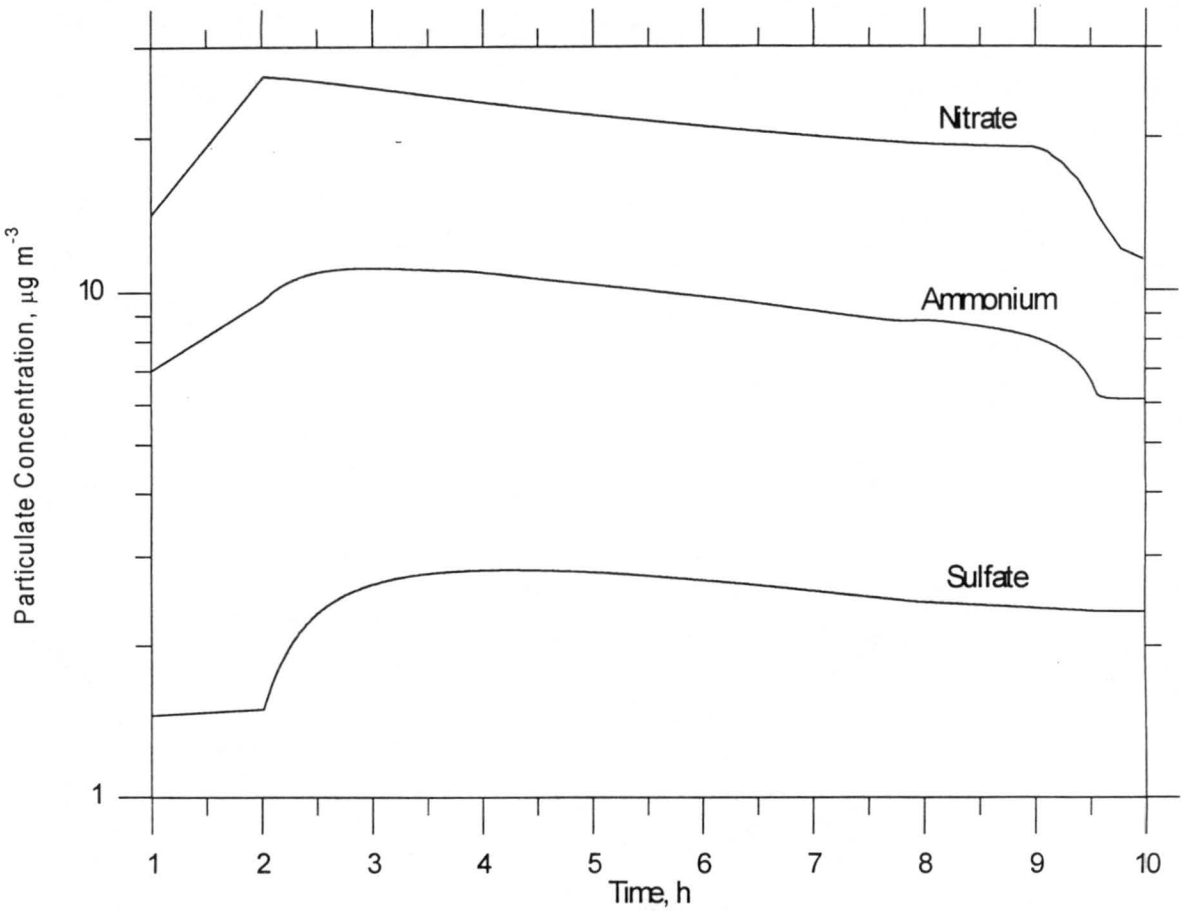

Figure 3.9. Evolution of the particulate (interstitial aerosol plus fogwater) concentrations of the major inorganic aerosol components during the fog episode of December 10, 1995 in Fresno.

An additional 2.5 μg m^{-3} of ammonia and 12.2 μg m^{-3} of nitrate are transferred to the particulate phase during this period. The production of sulfate is rather slow during this conditioning period because of the small availability of liquid water. The sulfate production increases dramatically around 2 a.m. as the fog starts and the liquid water content exceeds 0.2 g m^{-3}. At that stage most of the nitric acid that existed in the gas phase during the conditioning period has been transferred to the aqueous phase. The ammonium and nitrate concentrations start decreasing as fog droplets settle to the ground removing the corresponding ammonium nitrate. The concentration of particulate nitrate is reduced from a maximum of 26.3 μg m^{-3} to 18.8 μg m^{-3} at 8 a.m. A further reduction of nitrate follows as the RH decreases further shifting the equilibrium of ammonium nitrate towards the gas phase. The behavior of ammonia is qualitatively similar to nitrate as there are no aqueous-phase chemical sources or sinks. After the fog formation the ammonium

concentration decreases monotonically because of its wet removal. Removal of sulfate competes with aqueous-phase production throughout the fog episode resulting in a net increase of 60% in the sulfate concentration (final concentration = 2.3 μg m^{-3}). The reactions of S(IV) with ozone and hydrogen peroxide are responsible for this concentration increase.

The above results indicate that the current size-resolved chemistry model can successfully reproduce the major features of the SJV fog episode of December 10, 1995. In the subsequent paragraphs, they will therefore be used as diagnostic tools for the investigation of the role of aqueous-phase chemistry and wet removal during this episode.

3.2.5 Role of Size-Resolved Aqueous-Phase Chemistry

The effect of the size-resolved chemistry on the chemical transformations taking place inside the fog layer was investigated by directly comparing the results of the above size-resolved model with the size-resolved/bulk chemistry model of Gurciullo and Pandis (1997). The two models solve the same equations for the fog microphysics, but the bulk model adds the chemical components of the various droplet groups, creating a bulk sample, and then solves the aqueous-phase chemistry equations. The calculated changes are then partitioned back to the droplet spectrum according to the liquid water content. Therefore, the two models are similar, with size-resolved chemistry being their only difference. For example, both models predict the same evolution of the liquid water content (Figure 3.3) and droplet spectrum (Figure 3.2). They also use the full droplet spectrum for the calculation of the wet removal rates, so in a sense they are both employing a size-resolved wet removal scheme. These similarities of the two models allow us to focus only on the effect of the size-resolved aqueous-phase chemistry.

The predictions of the two models for nitrate and ammonium are practically identical (within 3% or less) because of the lack of important pH-dependent chemical transformations involving these species in the fog droplets. The small observed differences are indirect effects due to the sulfate transformations.

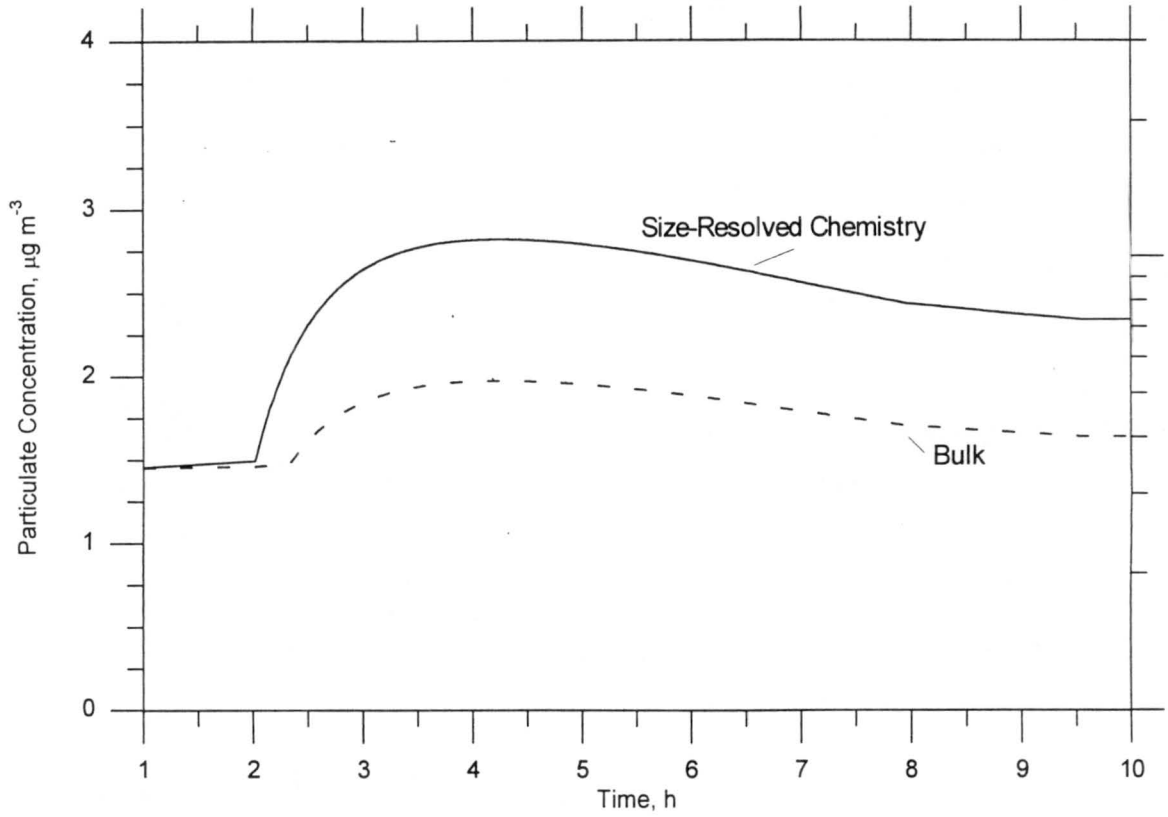

Figure 3.10. Predicted sulfate concentrations using a size-resolved and a bulk aqueous-phase chemistry model.

The bulk aqueous-phase chemistry model seriously underpredicts the sulfate formation rate from the ozone reaction. The final sulfate concentration predicted by the bulk approach is approximately 30% lower than that of the size-resolved model (Figure 3.10). This underprediction is sensitive to the ozone levels inside the fog layer. For the above simulation the ozone concentration inside the fog layer was kept constant at 5 ppb. According to the gas-phase chemistry module the lifetime of ozone for the observed NO levels is of the order of a few minutes. If the ozone is destroyed by NO and there are no additional ozone sources (for example entrainment from the fog top) then the size-resolved approach predictions are practically the same as those of the bulk approach.

3.2.6 Effect of Size-Resolved Chemistry on Wet Removal Rates

The CSU wet removal measurements indicated that the deposition velocity of ammonium was higher than that of sulfate which in turn exceeded the velocity of nitrate (Figure 3.11). One major weakness of fog models that do not account for the size distribution of

the droplets is that by default they predict the same deposition velocities for all species. According to the parameterization used this deposition velocity depends only on the fog liquid water content and not on the size distribution of the corresponding species. The deposition velocity predicted by the bulk fog model of Pandis and Seinfeld (1989b) for this fog episode is shown in Figure 3.11. It reaches a maximum value of 2.2 cm s^{-1} during the period of maximum fog liquid water content (4-6 a.m.).

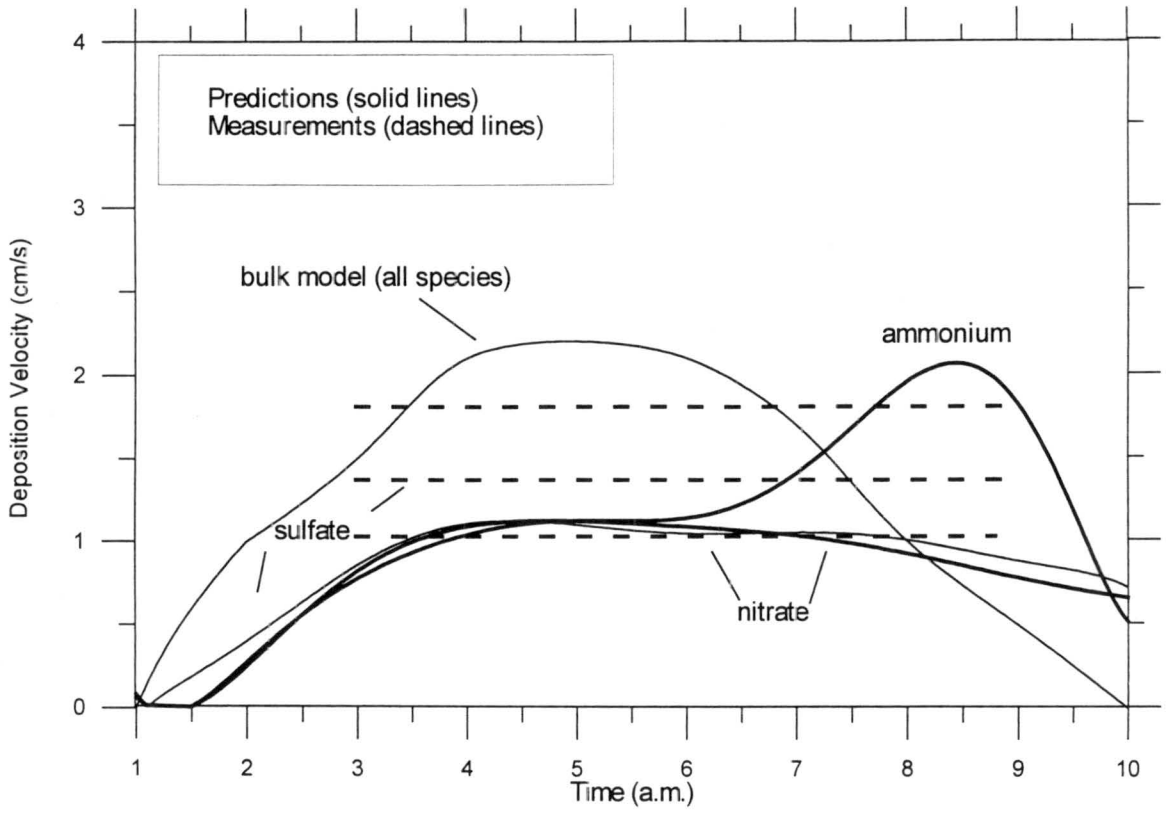

Figure 3.11. Predicted deposition velocities by the bulk model (all species), the size resolved model (solid lines) and measurements (dashed lines) during the December 10, 1995 fog episode.

The size-resolved model is able to reproduce the observed deposition velocities. It predicts a lower deposition velocity for nitrate, a result of its existence primarily in smaller droplets. Sulfate has a slightly higher deposition velocity as most of it is produced in droplets with sizes around 20 μm. Finally the ammonium deposition velocity is the highest, mainly due to an increase during the last 3-4 hours of the fog episode.

Because of the relatively high fog pH, ammonia is still available in the gas phase even after several hours of fog. This available ammonia has the time to be transferred to the larger fog droplets that in turn are removed faster. Nitric acid has been depleted from the gas phase during the fog formation stage and therefore does not show the same behavior. The mean predicted deposition velocities agree within 20-30% with the CSU measurements, providing further confidence about our ability to simulate the size-resolved fog processes during this fog episode.

4. Summary and Conclusions

San Joaquin Valley fogs are important processors of particulate matter, contributing to new aerosol mass formation as well as to particulate matter removal via droplet deposition. SJV fogs have the potential to increase aerosol sulfate concentrations but at the same time to cause reductions in the aerosol concentration of nitrate, organics, ammonium and sodium as well as in the total aerosol mass concentration.

Observations of fog composition during IMS95 reveal that droplet composition varies with drop size. All inorganic ion species measured were observed to be enriched in small drops relative to their large drop concentrations. Small drops were also consistently more acidic than large drops, although both large and small drops were generally less acidic than cloud and fog drops found in most environments.

Tests of the size-resolved fog chemistry model of Carnegie Mellon University revealed its ability to predict size-dependent fog drop compositions in close agreement with IMS95 observations made by Colorado State University. Although further comparisons should be made, requiring collection of additional data sets, these initial comparisons are quite encouraging and support the use of the model as a tool for investigating the role of SJV fogs as aerosol processors.

Direct analysis of the fog chemistry and microphysics observations indicates that aqueous sulfate formation is an important phenomenon in SJV fogs. Despite low ozone concentrations observed in conjunction with the fog events, calculations of expected oxidation rates in the collected fog samples reveal ozone to be the most important oxidant for sulfate production in the fogs. Ozone was determined to be the dominant S(IV) oxidant in 98% of the study samples with a pH greater than 6.0. Temporal analysis of sulfate production rates in the fogs indicates there is no general decline in oxidation rates over the course of an episode. Although one expects the drops to acidify rapidly as S(IV) is oxidized to sulfuric acid, accompanied by a precipitous decline in the rate of S(IV) oxidation by ozone, enough buffering capacity is apparently present in the system to keep

droplet pH values relatively high. This issue is addressed in more detail in the report for task 4.6.8.

Because the rate of aqueous S(IV) oxidation by ozone depends nonlinearly on the hydrogen ion concentration, it is inaccurate to predict sulfate formation rates in these fogs based on average droplet acidity. Calculated sulfate formation rates using observations of size-dependent drop chemistry reveal that failure to account for chemical heterogeneity among the droplet population can result in underprediction of the rate of sulfur oxidation by as much as a factor of nine. Enrichment of ion concentrations in small drops, which settle to the ground only slowly, also appears capable of reducing aerosol removal rates via droplet sedimentation relative to values one would predict from average droplet composition.

The CMU model including descriptions of aerosol and droplet microphysics, gas and aqueous-phase chemistry and deposition was used to study the transformation of aerosol to fog droplets and back to aerosol during IMS95. The sulfate produced during fog episodes favors the aerosol particles that have access to most of the fog liquid water which are usually the large particles. Aerosol scavenging efficiencies of around 60% are calculated for SJV fogs during IMS95.

Simulation of the extended fog event of December 10, 1995 indicated the fog contributes substantially to removal of ammonium and nitrate from the boundary layer. Removal of sulfate competes with aqueous-phase production throughout the fog episode resulting in a net increase of 60% in sulfate concentration. Sulfate production in the model is dominated by the ozone and hydrogen peroxide pathways. Simulation of the size-dependent fog drop composition results in a sulfate concentration that is 30% higher than predicted by a bulk fog model simulation of the same episode.

Sampling and subsequent mixing of fog droplets of different sizes may result in measured concentrations that are not fully representative of the fogwater chemical composition and can introduce errors in the reported values of the ionic species deposition velocities.

Differences in the major ionic species deposition velocities (ammonium > sulfate > nitrate) can be explained by their distribution over the fog drop size spectrum.

Because the effects of size-dependent drop composition are so important to aerosol formation and removal in fogs, it is recommended that future studies of winter particulate matter processing by SJV fogs consider this issue further. The encouraging agreement between model simulations and size-resolved fog chemistry observations suggest that a wise use of resources would be to make detailed measurements of size-resolved fog drop composition at a core location and rely on simpler measurements at other sites.

During IMS 95 we were fortunate that large changes in drop composition predicted by the CMU model coincided rather closely with the size cuts of the two size-fractionating collectors (sf-CASCC and ETH cloud impactor) deployed in the study. With recent advances in technology for measuring size resolved fog chemistry (CSU has successfully measured variations in fog drop acidity across 5 size fractions in a recent study in Davis, California), we recommend that greater drop size resolution be used for size-resolved drop chemistry measurements at a core site in a future SJV winter particulate matter study. These measurements should be accompanied by high time resolution fog drop size distribution and fog liquid water content measurements to test the model's simulation of fog microphysics and by fog deposition measurements to help constrain model simulations of solute flux to the ground via droplet sedimentation. In order to properly simulate the size-resolved fog chemistry, it is important that pre-fog measurements of the size-dependent aerosol composition (e.g., with a MOUDI or Berner impactor) also be made at this site. One or two additional satellite sites should be equipped with easy-to-operate two stage fog collectors. A two-stage strand collector (such as the size-fractionating Caltech Active Strand Cloudwater Collector, sf-CASCC) could be operated by a single fog site operator and would provide superior information to that available from a single-stage, bulk collector. Finally, if resources permit, it would be wise to add additional, automated sites employing single-stage strand collectors. If these stations were configured to collect one sample per fog event, several could be serviced by a roving fog operator that would visit the sites once per day. Such sites would provide

information about spatial variations in fog composition that were not examined during IMS95 (e.g., does fog along the western valley slope remain considerably more acidic than fog in the center of the valley, as observed during SJV fog studies conducted in the early 1980's). In order to permit data intercomparison, one and two-stage strand collectors should also be located at the core fog measurement site.

References

Bator A. and Collett J.L. Jr. (1997) Cloud chemistry varies with drop size. *J. Geophys Rev.* **102**, 28071-28078.

Boyce S.D., and Hoffmann M.R. (1984) Kinetics and mechanism of the formation of hydroxymethanesulfonic acid at low pH. *J. Phys. Chem.* **88**, 4740-4746.

Carter, W. P. L., F. W. Lurmann, R. Atkinson, and A. C. Lloyd (1986) Development and testing of a surrogate species chemical reaction mechanism. EPA-600/3-86-031.

Carter, W. P. L. and R. Atkinson (1988) Development and implementation of an up-to-date photochemical mechanism for use in airshed modeling, Summary final report to California Air Resources Board.

Cass, G. R. and F. H. Shair (1974) Sulfate accumulation in a sea breeze/land breeze circulation system, *J. Geophys. Res.*, **89**, 1429-1438.

Collett J.L. Jr., Bator A., Rao X. and Demoz B. (1994) Acidity variations across the cloud drop size spectrum and their influence on rates of atmospheric sulfate production. *Geophys. Rev. Lett.* **21**, 2393-2396.

Dollard, G. J. and M. H. Unsworth (1983) Field measurements of turbulent fluxes of wind-driven fog drops to a grass surface, *Atmos. Environ.*, **17**, 775-780.

Flossmann, A. I., W. D. Hall, and H. R. Pruppacher (1985) A theoretical study of the wet removal of amospheric pollutants. Part I: The redistribution of aerosol particles captured through nucleation and impaction scavenging by growing cloud drops, *J. Atmos. Sci.*, **42**, 583-606.

Flossmann, A. I., H. R. Pruppacher, and J. H. Topalian (1987) A theoretical study of the wet removal of atmospheric pollutants. Part II: The uptake and redistribution of $(NH_4)_2SO_4$ particles and SO_2 gas simultaneously scavenged by growing cloud drops, *J. Atmos. Sci.*, **44**, 2912-2923.

Gurciullo C. S. and S. N. Pandis (1997) Effects of composition variations in cloud droplet populations on aqueous-phase chemistry, *J. Geophys. Res.*, **102**, 9375-9385.

Hegg, D. A. and T. V. Larson (1990) The effects of microphysical parameterization on model predictions of sulfate production in clouds, *Tellus*, **42B**, 272-284.

Hoffmann M. R. (1986) On the kinetics and mechanism of oxidation of aquated sulfur dioxide by ozone. *Atmos. Environ.* **20**, 1145-1154.

Ibusuki T. and Takeuchi K. (1987) Sulfur dioxide oxidation by oxygen catalyzed by mixtures of manganese (II) and iron (III) in aqueous solutions at environmental reaction conditions. *Atmos. Environ.* **21**, 1555-1560.

Jensen, J. B. and R. J. Charlson (1984) On the efficiency of nucleation scavenging, *Tellus*, **36B**, 367-375.

Kok G.L., Gitlin S.N. and Lazrus A.L. (1986) Kinetics of the formation and decomposition of hydroxymethanesulfonate. *J. Geophys. Res.* **91**, 2801-2804.

Lillis D., Cruz C. N., Collett Jr. J. L., Richards L. W. and Pandis S. N. (1998) Production and removal of aerosol in a polluted fog layer. *Atmos Environ.*, submitted.

Munger J.W., Jacob D.J., Waldman J.M. and Hoffmann, M.R. (1983) Fogwater chemistry in an urban atmosphere. *J. Geophys. Rev.* **88**, 5109-5121.

Munger, J. W., J. Collett, B. Daube, and M. R. Hoffmann (1990) Fogwater chemistry at Riverside, California, *Atmos. Environ.*, **24B**, 182-205.

Olson T.M. and Hoffmann M.R. (1986) On the kinetics of formaldehyde-S(IV) adduct formation in slightly acidic solution. *Atmos. Environ.* **20**, 2277-2278.

Olson T.M. and Hoffmann M.R. (1989) Hydroxymethanesulfonate formation: Its role as a S(IV) reservoir in atmospheric water droplets. *Atmos. Environ.* **23**, 985-997.

Pandis, S. N. and J. H. Seinfeld (1989a) Sensitivity analysis of a chemical mechanism for aqueous-phase atmospheric chemistry, *J. Geophys. Res.*, **94**, 1105-1126.

Pandis, S. N. and J. H. Seinfeld (1989b) Mathematical modeling of acid deposition due to radiation fog, *J. Geophys. Res.*, **94**, 12911-12923.

Pandis, S. N., C. Pilinis, and J. H. Seinfeld (1990a) The smog-fog-smog cycle and acid deposition, *J. Geophys. Res.*, **95**, 8489-8500.

Pandis, S. N., J. H. Seinfeld, and C. Pilinis (1990b) Chemical composition differences in fog and cloud droplets of different sizes, *Atmos. Environ.*, **24A**, 1957-1969.

Pilinis, C. and J. H. Seinfeld (1987) Continued development of a general equilibrium model for inorganic multicomponent atmospheric aerosols, *Atmos. Environ.*, **21**, 2453-2466.

Pilinis, C. and J. H. Seinfeld (1988) Development and evaluation of an Eulerian photochemical gas-aerosol model, *Atmos. Environ.*, **22**, 1985-2001.

Pruppacher, H. R. and J. D. Klett (1980) *Microphysics of clouds and precipitation*, Reidel Pub. Co., The Netherlands.

Rao X. and Collett J.L. Jr. (1995) The behavior of S(IV) and formaldehyde in a chemically heterogeneous cloud. *Environ. Sci. Tech.* 29, 1023-1031.

Rao X. and Collett J.L. Jr. (1998) The drop size-dependence of iron and manganese concentrations in clouds and fogs: implications for sulfate production. *J. Atmos. Chem. 30, 273-289.*

Seinfeld J.H. (1986) *Atmospheric Chemistry and Physics of Air Pollution.* Wiley, New York.

Ten Brink, H. M., S. E. Schwartz and Daum, P. H. (1987) Efficient scavenging of aerosol sulfate by liquid water clouds, *Atmos. Environ.*, **21**, 2035-2052.

Waldman J. M (1986) Depositional aspects of pollutant behavior in fog, Ph.D. Thesis, Caltech, Pasadena.

Waldman, J. M. and Hoffmann, M. R. (1987) Sources and Fates of Aquatic Pollutants, in ACS Advances in Chemistry Series No. 216, R. A. Hites and S. J. Eisenreich Eds.; American Chemical Society, New York, pp. 79-129.

Warren, D. R. and J. H. Seinfeld (1985) Simulation of aerosol size-distribution evolution in systems with simultaneous nucleation, condensation and coagulation, *Aerosol Sci. Technol.*, **4**, 31-43.

Wilkins, E. T. (1954) Air pollution aspects of the London fog of December 1952, *J. R. Meteorol. Soc.*, **80**, 267-278.